SIAM J. SCI. COMPUT.
Vol. 32, No. 2, pp. 603–634
© 2010 Society for Industrial and Applied Mathematics

FLUID SOLVER INDEPENDENT HYBRID METHODS FOR MULTISCALE KINETIC EQUATIONS*

GIACOMO DIMARCO† AND LORENZO PARESCHI‡

Abstract. In some recent works [G. Dimarco and L. Pareschi, *Comm. Math. Sci.*, 1 (2006), pp. 155–177; *Multiscale Model. Simul.*, 6 (2008), pp. 1169–1197] we developed a general framework for the construction of hybrid algorithms which are able to face efficiently the multiscale nature of some hyperbolic and kinetic problems. Here, in contrast to previous methods, we construct a method form-fitting to any type of finite volume or finite difference scheme for the reduced equilibrium system. Thanks to the coupling of Monte Carlo techniques for the solution of the kinetic equations with macroscopic methods for the limiting fluid equations, we show how it is possible to solve multiscale fluid dynamic phenomena faster than using traditional deterministic/stochastic methods for the full kinetic equations. In addition, due to the hybrid nature of the schemes, the numerical solution is affected by fewer fluctuations than are standard Monte Carlo schemes. Applications to the Boltzmann-BGK equation are presented to show the performance of the new methods in comparison with classical approaches used in the simulation of kinetic equations.

Key words. multiscale problems, hybrid methods, Boltzmann-BGK equation, Euler equation, Monte Carlo methods, fluid dynamic limit

AMS subject classifications. 65M99, 65L06, 82D05

DOI. 10.1137/080730585

1. Introduction.

The classical fluid dynamic models like the Navier–Stokes or Euler equations are not always satisfactory when dealing with large temperatures or very low densities, and a more detailed analysis often becomes necessary to obtain correct values of the macroscopic quantities. In such cases a kinetic approach based on the Boltzmann equation [6] is used. The introduction of such a model is closely linked with the introduction of serious difficulties from the numerical and computational point of view. In fact, the system of equations to be solved becomes very large, especially in multidimensional situations, and even with computers of the last generation the computational cost of a direct discretization is often prohibitive. Moreover, the Boltzmann collision term that characterizes the kinetic equation is very hard to treat in practice due to its nonlinear nature and physical properties. For these reasons, probabilistic techniques such as direct simulation Monte Carlo (DSMC) are extensively used in real simulations for their great flexibility, capability of treating different collision terms, and low computational cost compared to deterministic schemes for kinetic equations [2, 4, 21, 23]. On the other hand, solutions are affected by large fluctuations, and, in nonstationary situations, the difficulty of computing averaged quantities leads to low-accuracy solutions or very expensive simulations. However, even in extremely rarefied regimes the fluid dynamic equations still furnish correct solution in regions of the domain where the gas is not subjected to a sharp gradient. The

*Received by the editors July 17, 2008; accepted for publication (in revised form) November 4, 2009; published electronically February 17, 2010. This work was partially supported by the INDAM project "Kinetic Innovative Models for the Study of the Behavior of Fluids in Micro/nano Electromechanical Systems."

http://www.siam.org/journals/sisc/32-2/73058.html

†Institut de Mathématiques de Toulouse, Equipe "Mathématiques pour l'Industrie et la Physique," CNRS, Université Paul Sabatier, Toulouse 1, Toulouse 2 et INSA Toulouse, Unité Mixte 5219, 118 Route de Narbonne, 31062 Toulouse Cedex, France (dmrgcm@unife.it).

‡Department of Mathematics and CMCS, University of Ferrara, 35 via Machiavelli, 44100 Ferrara, Italy (Lorenzo.Pareschi@unife.it).

Copyright © by SIAM. Unauthorized reproduction of this article is prohibited.

direct consequence is that domain decomposition methods [3, 20, 10] which consider the problem at different scales, fluid or kinetic, in different part of the computational domain, are a practical way to take advantage of the physics without losing accuracy. We note also the possibility of improving domain decomposition schemes through a moving boundary [9, 33], in order to follow discontinuities and sharp gradients inside the domain; these methods are particularly important in the simulation of nonstationary problems. Clearly, the exact identification of the nonequilibrium zones remains a hard task to deal with and an open research area.

In some recent works we proposed an alternative approach to domain decomposition methods based on the use of different numerical methods on the whole computational domain [12, 13]. We mention here that similar hybrid approaches have been considered in [8, 15, 16, 23, 32]. Even if we develop our methods in the case of rarefied gas dynamics (RGD), the formulation we propose easily permits generalizations to others fields in which kinetic and hyperbolic multiscale phenomena are present. In order to use the hybrid approach described here, it is essential to identify a local equilibrium function, like the Maxwellian distribution for RGD, either analytically or numerically. This local equilibrium originates a model reduction from the microscale to the macroscale formulation and allows us to ignore the details of microscopic interactions in terms of simplified equations which describe the equilibrium system.

The schemes presented here represent an important improvement with respect to the schemes developed in [12, 13], where the limiting equilibrium method was limited by construction to a kinetic scheme. In the present work we generalize the approach to make the method independent of the fluid solver used. We point out that this generalization is not trivial, since in an arbitrary fluid solver we miss the kinetic information on the distribution function which is present in a standard kinetic scheme. The main advantage is that the method in the fluid limit degenerates into a standard fluid solver without any additional cost for a kinetic simulation. To our knowledge this is the first method which satisfies this property for RGD.

Although we will focus, in the construction of the schemes, on the simplified Bhatnagar–Gross–Krook (BGK) collision model [1], in principle the schemes can be extended to the full Boltzmann collision operator through the use of time relaxed Monte Carlo methods [22, 23, 24, 25]. The basic idea consists of solving the kinetic and macroscopic models in the entire domain, the first through Monte Carlo techniques which are robust in the fluid limit, and the latter through a deterministic scheme, and then considering as a solution a suitable hybrid merging of the two. A remarkable feature of this new method is the use of the hybrid moments to correct the stochastic moments in the pure Monte Carlo scheme. This is an important source of fluctuation reduction in the method.

In addition we will show that it is not necessary to keep the number of sample particles fixed in the Monte Carlo scheme, since it is sufficient to describe at the particle level only the fraction of the solution which is far from the thermodynamic equilibrium. An immediate consequence of the above observation is a potential reduction of the number of samples used in the Monte Carlo solution and, thereby, of computational time and fluctuations. These improvements are directly linked with the decrease of the local Knudsen number, which is a measure of the rarefaction of the gas. The implementation of such a methodology produces numerical schemes which, in general, are much faster than deterministic kinetic schemes and, for flow regimes close to the fluid limit, also than DSMC schemes. Moreover, thanks to the general for-

Copyright © by SIAM. Unauthorized reproduction of this article is prohibited.

mulation of the algorithm, a domain decomposition technique can be directly derived forcing the Knudsen number to zero (see [14]) in some regions of the domain.

Finally, let us observe that the method here developed is based on the classical operator splitting for the kinetic equation. This is essential if one wants to match the fluid scheme with standard DSMC solvers for RGD, since the latter are based on such splitting. Even if there are well-known limitations of such splitting when dealing with Navier–Stokes asymptotics, since the time step has to be related to the Knudsen number in order to describe correctly the Navier–Stokes level [34], here we do not aim at an underresolved method at all scales, but simply at developing a method which is asymptotic preserving (AP) in the stiff limit [17]. On the other hand, the advantages provided by our final method in terms of fluctuations and computational cost reduction are essentially independent of the small scale resolution but depend only on the Knudsen number. Note that in principle one can improve the method by coupling the DSMC solver with a Navier–Stokes fluid description instead of an Euler one. This coupling, however, is not straightforward, and we do not explore this direction here.

The rest of the article is organized as follows. In section 2 we introduce the BGK equations and their properties. In section 3 we recall the general structure of the hybrid methods derived in [12, 13]. Next in section 4 the fluid solver independent (FSI) hybrid scheme is described together with an acceleration technique and two possible ways in which the equilibrium fraction can be increased. Section 5 is devoted to numerical results, comparing the performance of our method with those of the traditional Monte Carlo and kinetic schemes. Some final considerations and future developments are discussed in the last section.

2. The Boltzmann-BGK model. We consider the following Boltzmann-BGK kinetic model:

$$\partial_t f(x,v,t) + v \cdot \nabla_x f(x,v,t) = \frac{1}{\tau(x,t)}(M_f(x,v,t) - f(x,v,t)), \tag{2.1}$$

with the initial condition

$$f(x,v,t=0) = f_0(x,v). \tag{2.2}$$

In (2.1) the function $f(x,v,t)$ is nonnegative and describes the time evolution of the distribution of particles with velocity $v \in \mathbb{R}^d$ and position $x \in \Omega \subset \mathbb{R}^D$, where d and D are the dimension in velocity and physical space, respectively. In this simplified model the Boltzmann collision term is substituted by a relaxation towards equilibrium. In what follows we will work with nondimensional quantities so that the relaxation frequency τ can be written as

$$\tau(x,t)^{-1} = \frac{C}{\varepsilon(x,t)}, \tag{2.3}$$

where $\varepsilon(x,t)$ is the Knudsen number. Here we assume $C = 1$ (see [7, 30]). Other choices for the relaxation time do not change the hybrid algorithm that we will describe in the next section. Observe anyway that the ratio of deterministic and stochastic components will be a function of the relaxation time, being linked to the ratio of the distribution function with respect to the Maxwellian equilibrium function, as explained in detail in the next section. In the following, for simplicity, we will skip the space- and time dependency on the Knudsen number; thus $\varepsilon(x,t) = \varepsilon$.

Copyright © by SIAM. Unauthorized reproduction of this article is prohibited.

The local Maxwellian function, representing the local equilibrium, is defined by

$$M_f(\varrho, u, T)(x, v, t) = \frac{\varrho}{(2\pi T)^{d/2}} \exp\left(\frac{-|u-v|^2}{2T}\right), \tag{2.4}$$

where ϱ, u, T are the density, mean velocity, and temperature of the gas in the x-position, and at time t

$$\varrho = \int_{\mathbb{R}^d} f dv, \quad u = \frac{1}{\varrho}\int_{\mathbb{R}^d} v f dv, \quad T = \frac{1}{d\varrho}\int_{\mathbb{R}^d} |v-u|^2 f dv, \tag{2.5}$$

while the energy E is defined as

$$E = \frac{1}{2}\int_{\mathbb{R}^d} |v|^2 f dv. \tag{2.6}$$

Consider now the BGK equation (2.1) and multiply it by the so-called collision invariants 1, v, and $\frac{1}{2}|v|^2$. By integrating in v the above quantities, the equations for the first three moments of the distribution function f are obtained. They describe respectively the conservations laws for mass, momentum, and energy. Unfortunately, the system obtained through the above average in velocity space is not closed since it involves higher order moments of the distribution function.

Note that, formally from (2.1) as $\varepsilon \to 0$, the function f approaches the local Maxwellian. In this case it is possible to compute analytically the higher moments of f from ϱ, u, and T. Carrying on this computation, we obtain the set of compressible Euler equations (see [5] for details)

$$\begin{aligned} &\frac{\partial \varrho}{\partial t} + \nabla_x \cdot (\varrho u) = 0, \\ &\frac{\partial \varrho u}{\partial t} + \nabla_x \cdot (\varrho u \otimes u + p) = 0, \\ &\frac{\partial E}{\partial t} + \nabla_x \cdot (Eu + pu) = 0, \\ &p = \varrho T, \qquad E = \frac{d}{2}\varrho T + \frac{1}{2}\varrho |u|^2, \end{aligned} \tag{2.7}$$

where p is the thermodynamical pressure while $\otimes$ represents a tensor product. A higher order fluid model, like Navier–Stokes, can be derived similarly [5].

3. Hybrid methods. The schemes derived in this paper are based on the same hybrid representation defined in [13]. Here we recall only the key points of the previous method; for details we refer the reader to [13].

For a fixed space point x we can interpret the distribution function as a probability density in the velocity space (the x-dependence is omitted),

$$f(v,t) \geq 0, \quad \varrho = \int_{-\infty}^{+\infty} f(v,t) dv = 1. \tag{3.1}$$

Next we recall the following definition of hybrid representation [13].

DEFINITION 3.1. *Given a probability density $f(v,t)$ and a probability density $M_f(v,t)$, called the equilibrium density, we define $w(v,t) \in [0,1]$ and $\tilde{f}(v,t) \geq 0$ in the following way:*

$$w(v,t) = \begin{cases} \dfrac{f(v,t)}{M_f(v,t)}, & f(v,t) \leq M_f(v,t) \neq 0, \\ 1, & f(v,t) \geq M_f(v,t), \end{cases} \tag{3.2}$$

Copyright © by SIAM. Unauthorized reproduction of this article is prohibited.

and

$$\tilde{f}(v,t) = f(v,t) - w(v,t)M_f(v,t). \tag{3.3}$$

Thus $f(v,t)$ can be represented as

$$f(v,t) = \tilde{f}(v,t) + w(v,t)M_f(v,t). \tag{3.4}$$

If we now take $\beta(t) = \min_v\{w(v,t)\}$ and $\tilde{f}(v,t) = f(v,t) - \beta(t)M_f(v,t)$, we have

$$\int_v \tilde{f}(v,t)dv = 1 - \beta(t).$$

Let us define for $\beta(t) \neq 1$ the probability density

$$f^p(v,t) = \frac{\tilde{f}(v,t)}{1-\beta(t)}.$$

The case $\beta(t) = 1$ is trivial since it implies $f(v,t) = M_f(v,t)$. Thus the probability density $f(v,t)$ can be written as a convex combination of two probability densities in the form [22, 23]

$$f(v,t) = (1-\beta(t))f^p(v,t) + \beta(t)M_f(v,t). \tag{3.5}$$

Clearly the above representation is a particular case of (3.4).

Now we consider the following general representation, including space dependence:

$$f(x,v,t) = \tilde{f}(x,v,t) + w(x,v,t)M_f(x,v,t), \tag{3.6}$$

where $w(x,v,t) \geq 0$ is a function characterizing the equilibrium fraction and $\tilde{f}(x,v,t)$ the nonequilibrium part of the distribution function. This representation can in general be obtained for the initial data of the kinetic equation by directly using Definition 3.1.

The starting point of the method is the classical operator splitting, which consists of solving first a homogeneous relaxation step

$$\partial_t f^r(x,v,t) = -\frac{1}{\varepsilon}(f^r(x,v,t) - M^r(x,v,t)) \tag{3.7}$$

and then a free transport equation

$$\partial_t f^c(x,v,t) + v \cdot \nabla_x f^c(x,v,t) = 0. \tag{3.8}$$

In a single time step Δt the computation of the hybrid method derived in [13] can be summarized as follows.

- Starting from a function $f^r(x,v,t) = f(x,v,t)$ in the form (3.6), solve the relaxation step (3.7) either analytically or with a suitable numerical time integrator for stiff ODEs, like backward Euler. This originates the decomposition

$$\begin{aligned} f^r(x,v,t+\Delta t) &= \lambda f^r(x,v,t) + (1-\lambda)M_f(x,v,t) \\ &= \lambda\tilde{f}(x,v,t) + (1-\lambda+\lambda w(x,v,t))M_f(x,v,t), \end{aligned}$$

  with $0 \leq \lambda = \lambda(\Delta t/\varepsilon) \leq 1$ a scheme dependent constant such that $\lambda \to 0$ as $\Delta t/\varepsilon \to \infty$. This decomposition can be cast again in the form (3.6), taking $\tilde{f}^r(x,v,t+\Delta t) = \lambda\tilde{f}(x,v,t)$ and $w^r(x,v,t+\Delta t) = 1-\lambda+\lambda w(x,v,t)$.

Copyright © by SIAM. Unauthorized reproduction of this article is prohibited.

1. The new value $w^r(x, v, t + \Delta t)$ follows directly from the choice of λ, and thus from the time solver used for (3.7).
2. The new value $\tilde{f}^r(x, v, t + \Delta t)$ is computed by a Monte Carlo method, simply discarding a fraction of the samples since $0 \leq \lambda \leq 1$ and so $w^r(x, v, t + \Delta t) \geq w(x, v, t)$.

- Starting from the function $f^c(x, v, t) = f^r(x, v, t + \Delta t)$ in the form (3.6) computed above, solve the transport step (3.8).
  1. Transport the particle fraction $\tilde{f}^c(x, v, t)$ by simple particles shifts.
  2. Transport the deterministic fraction $w^c(x, v, t)M_f(x, v, t)$ by a deterministic scheme.
  3. Project the computed hybrid solution $f(x, v, t + \Delta t)$ to the form (3.6) using Definition 3.1.

Clearly point 3 of the transport step is crucial for the details of the hybrid method. Note that point 2 of the transport step involves the solution of a so-called kinetic scheme for the Euler equations [11, 28].

In what follows we will describe the FSI schemes which remove the limitations given by the use of a kinetic scheme. One major difference from the hybrid scheme described above is that a common value for the equilibrium fraction in velocity space has to be chosen, $\beta(x, t) = \min_v\{w(x, v, t)\}$.

4. FSI hybrid methods. The key feature of FSI methods is that they take advantage of the solution of the equilibrium part of the distribution function through a macroscopic scheme instead of a kinetic one. Besides its generality, this new feature could, in principle, lead to a strong reduction of the computational time as compared to any kinetic scheme for the fluid equation.

In order to describe the FSI method we introduce the projection operator $\mathcal{P}$, and, in a time step Δt, the relaxation operator $\mathcal{R}_{\Delta t}$ and the transport operator $\mathcal{T}_{\Delta t}$. The projection operator computes the macroscopic averages $U(x, t) = (\varrho(x, t), \rho u(x, t), E(x, t))$ from the kinetic variable f (or M_f), so that

$$\mathcal{P}(f(x, v, t)) = U(x, t), \quad \mathcal{P}(M_f(x, v, t)) = U(x, t), \tag{4.1}$$

since the local Maxwellian M_f has the same moments of the distribution function f. The relaxation and transport operators solve the relaxation and transport steps. The first has the form

$$\mathcal{R}_{\Delta t}(f(x, v, t)) = \lambda f(x, v, t) + (1 - \lambda)M_f(x, v, t), \tag{4.2}$$

where $\lambda = \exp(-\Delta t/\varepsilon)$, whereas the second reads

$$\mathcal{T}_{\Delta t}(f(x, v, t)) = f(x - v\Delta t, v, t). \tag{4.3}$$

In addition, we have the approximated relaxation and transport operators $\mathcal{R}_a$ and $\mathcal{T}_a$. For simplicity, since their particular structure does not play any role in the general derivation of the method, we assume in what follows that $\mathcal{T}_a = \mathcal{T}$ and $\mathcal{R}_a = \mathcal{R}$. Note that $\mathcal{P}(\mathcal{R}_{\Delta t}(M_f)) = \mathcal{P}(M_f)$ because, by definition, $\mathcal{R}_{\Delta t}(M_f) = M_f$.

4.1. A simple FSI method. Let us start from a hybrid solution in the form

$$f(x, v, t) = (1 - \beta(x, t))f^p(x, v, t) + \beta(x, t)M_f(x, v, t), \tag{4.4}$$

where $f^p(x, v, t)$ is represented by samples so that

$$(1 - \beta(x, t))f^p(x, v, t) = m^p \sum_{j=1}^{N(t)} \delta(x - p_j(t))\delta(v - \nu_j(t)), \tag{4.5}$$

Copyright © by SIAM. Unauthorized reproduction of this article is prohibited.

where $p_j(t)$ and $\nu_j(t)$ represent the particles position and velocity and

$$m^p = \frac{1}{N(0)} \int_{\mathbb{R}^d} \int_{\mathbb{R}^D} f(x, v, 0) dx dv$$

is the mass of a single particle, while $M_f(x, v, t)$ is represented analytically. Note that $N(t)$, namely the total number of samples, is a function of time since we keep m^p constant during the simulation. This is a crucial feature of the method since if we increase $\beta(x, t)$ in the representation above, we must decrease the number of samples $N(t)$. In practice this implies that we will not be able to represent exactly the fraction $\beta(x, t)$ but only its approximation corresponding to integer sums of particles.

Since, as described in the previous section, the first relaxation step has only the consequence of a change of $\beta(x, t)$ in (4.4), we derive the method starting from the transport step.

The transport step produces the solution

$$\mathcal{T}_{\Delta t}(f(x, v, t)) = (1 - \beta(x - v\Delta t, t)) f^p(x - v\Delta t, v, t) + \beta(x - v\Delta t, t) M_f(x - v\Delta t, v, t).$$

From a practical viewpoint $(1 - \beta(x - v\Delta t, t)) f^p(x - v\Delta t, v, t)$ corresponds to solving a simple particle shift for the Monte Carlo samples. At variance the term $\beta(x - v\Delta t, t) M_f(x - v\Delta t, v, t)$ corresponds to a Maxwellian shift analogous to that usually performed in the so-called kinetic or Boltzmann schemes for the Euler equations [11, 28]. The hybrid solution for the moments $U^H(x, t + \Delta t)$ is then recovered as

$$\begin{aligned} U^H(x, t + \Delta t) &= \mathcal{P}(\mathcal{T}_{\Delta t}(f(x, v, t))) \\ &= \mathcal{P}(\mathcal{T}_{\Delta t}((1 - \beta(x, t)) f^p(x, v, t))) + \mathcal{P}(\mathcal{T}_{\Delta t}(\beta(x, t) M_f(x, v, t))) \\ &= U^p(x, t + \Delta t) + U^K(x, t + \Delta t). \end{aligned}$$

In particular, $U^K(x, t + \Delta t)$ corresponds exactly to the approximation of the Euler solution provided by a kinetic/Boltzmann scheme.

We can now state the following result (see also [29]).

THEOREM 4.1. *If we denote by $U^E(x, t + \Delta t)$ the solution of the Euler equations* (2.7) *with initial data $U^E(x, t) = \mathcal{P}(\beta(x, t) M_f(x, v, t))$, we have*

$$U^E(x, t + \Delta t) = U^K(x, t + \Delta t) + O(\Delta t^2). \tag{4.6}$$

Proof. In a time step Δt we can write for the Euler solution

$$U^E(x, t + \Delta t) = U^E(x, t) + \Delta t \partial_t U^E(x, t) + \frac{1}{2} (\Delta t)^2 \partial_{tt} U^E(x, t) + O(\Delta t^3)$$

and similarly

$$U^K(x, t + \Delta t) = U^K(x, t) + \Delta t \partial_t U^K(x, t) + \frac{1}{2} (\Delta t)^2 \partial_{tt} U^K(x, t) + O(\Delta t^3).$$

Clearly the zero order terms in the expansions are the same since the initial data of the Euler equations is simply the projection of the initial data for the transport equation

$$U^K(x, t) = \mathcal{P}(\beta(x, t) M_f(x, v, t)) = U^E(x, t).$$

Now let us consider the first order terms. We have

$$\partial_t U^E = -(\nabla_x \cdot (\varrho u), \nabla_x \cdot (\varrho u \otimes u + p), \nabla_x \cdot (Eu + pu))^T$$

Copyright © by SIAM. Unauthorized reproduction of this article is prohibited.

and

$$\partial_t U^K = \mathcal{P}(-v \cdot \nabla_x f).$$

Note that this last equation is not closed since the right-hand side involves third order moments of f. Again, however, the two terms evaluated at the initial time t coincide since the initial data for the transport step is the Maxwellian fraction $\beta(x,t)M_f(x,v,t)$, and so we have the usual Euler closure in the kinetic term. By similar arguments one can verify that the second order terms evaluated at the initial time are different because of the fourth order moments appearing in $\partial_{tt}U^K(x,t) = \mathcal{P}(v \cdot \nabla_x(v \cdot \nabla_x f))$. This proves (4.6). ∎

By virtue of the above result we can replace the hybrid solution for the moments after the transport with

$$\tilde{U}^H(x,t+\Delta t) = U^p(x,t+\Delta t) + U^E(x,t+\Delta t), \tag{4.7}$$

without affecting the overall first order accuracy of the splitting method.

These hybrid values for the moments are used to compute the new Maxwellian $M_f^H(x,v,t+\Delta t)$ and advance the computation. To this end we note that the next relaxation step takes the form

$$\begin{aligned}
\mathcal{R}_{\Delta t}(\mathcal{T}_{\Delta t}(f(x,v,t))) &= \lambda \mathcal{T}_{\Delta t}(f(x,v,t)) + (1-\lambda)M_f^H(x,v,t+\Delta t) \\
&= \lambda(\mathcal{T}_{\Delta t}((1-\beta(x,t))f^p(x,v,t)) + \mathcal{T}_{\Delta t}(\beta(x,t)M_f(x,v,t))) \\
&\quad + (1-\lambda)M_f^H(x,v,t+\Delta t) \\
&= (1-\beta(x,t+\Delta t))f^p(x,v,t+\Delta t) + \beta(x,t+\Delta t)M_f^H(x,v,t+\Delta t),
\end{aligned}$$

where we set

$$\beta(x,t+\Delta t) = 1-\lambda, \qquad f^p(x,v,t+\Delta t) = \mathcal{T}_{\Delta t}(f(x,v,t)) \tag{4.8}$$

with $\lambda = e^{-\Delta t/\varepsilon}$. This shows that in order to compute the new particle fraction we need to sample particles from $\mathcal{T}_{\Delta t}(\beta(x,t)M_f(x,v,t))$. In practice this can be realized in a simple way by initially transforming the equilibrium Maxwellian part $\beta(x,t)M_f(x,v,t)$ into samples and then advecting the whole set of samples.

Let us denote by $\mathcal{T}_{\Delta t}(\beta(x,t)M_f^p(x,v,t))$ this set of advected equilibrium samples. Computationally this means that at each time step me must solve the full BGK model with a Monte Carlo scheme [13] together with a suitable deterministic solver for the Euler equation. We can improve the efficiency of the above algorithm by observing that it is not necessary to transform the whole Maxwellian part into samples, but only a fraction $\bar{\lambda}$ of it, where

$$\bar{\lambda} \geq \max_x\{\lambda(x,t+\Delta t)\}.$$

As discussed before, the reason for this is that we know that at the subsequent relaxation step a fraction $\beta(x,t+\Delta t)$ of samples will be discarded in each cell. Thus we need only

$$(1-\beta(x,t+\Delta t))\mathcal{T}_{\Delta t}(\beta(x,t)M_f^p(x,v,t)) = \lambda(x,t+\Delta t)\mathcal{T}_{\Delta t}(\beta(x,t)M_f^p(x,v,t))$$

advected Maxwellian particles, which is guaranteed if in any cell before advection we have at least $\bar{\lambda}\beta(x,t)M_f^p(x,v,t)$ particles, since

$$\mathcal{T}_{\Delta t}(\bar{\lambda}\beta(x,t)M_f^p(x,v,t)) = \bar{\lambda}\mathcal{T}_{\Delta t}(\beta(x,t)M_f^p(x,v,t)).$$

Copyright © by SIAM. Unauthorized reproduction of this article is prohibited.

This is of paramount importance since $\bar{\lambda}$ vanishes as $\varepsilon/\Delta t \to 0$, and so the number of samples effectively used by the hybrid method is a decreasing function of the ratio between the Knudsen number and the time step.

Starting from initial data represented by particles, a simple FSI hybrid scheme for the solution of the BGK equation with λ constant in space and time is described in the following algorithm.

ALGORITHM 1 (FSI hybrid scheme).

1. *Compute the initial velocity and position of the particles* $\{\nu_j^0, j = 1, \dots, N\}$ $\{p_j^0, j = 1, \dots, N\}$ *by sampling them from initial density* $f_0(x, v)$. *Set* $m^p = \int\int f_0(x, v)dxdv/N$.
2. *Given a mesh* x_i, $i = 1, \dots, L$, *with grid size* Δx, *and an estimate of the larger sample velocity* $\nu_{max} = 4\sqrt{2T_{max}}$, *with* T_{max} *the maximum temperature, set* $\Delta t^p = \Delta x/\nu_{max}$.
3. *Compute the initial values of the moments of the distribution function in each cell* ϱ_i, $(\varrho u)_i$, E_i, $i = 1, \dots, L$.
4. *Compute the larger time step allowed by the deterministic macroscopic scheme* Δt_D.
5. *Set* $\Delta t = \min(\Delta t^p, \Delta t_D)$.
6. *Set* $n = 0$, $t = 0$, $\lambda = e^{-\Delta t/\varepsilon}$, $\bar{\lambda} = \lambda$, $\beta_i = 1 - \bar{\lambda}$, $i = 1, \dots, L$.
7. *While* $t \le t_f$ *with* t_f *the final chosen time, do the following:*
   (a) *Estimate the number of Maxwellian samples we need by using* $\bar{\lambda}\beta(x, t)M_f^p(x, v, t)$.
      i. *In each cell set* $N_i^M = \text{Iround}(\bar{\lambda}\beta_i\rho_i^n/(m^p/\Delta x))$ *and sample* N_i^M *equilibrium particles from the Maxwellian with moments* $(\rho u)_i^n, E_i^n$.
   (b) *Perform the transport step, keeping track of the particles that come from the above sampling.*
      i. *Transport all particles*

$$p_j^{n+1} = p_j^n + \nu_j^n \Delta t \quad \forall\, j. \tag{4.9}$$

      ii. *Compute the moments* $U_i^{p,n+1}$ *and the number of particles* N_i^p *in each cell using only the advected particles not sampled from the Maxwellian.*
      iii. *Solve the Euler equations for* $U_i^{E,n} = \beta_i U_i^n$, *and find* $U_i^{E,n+1}$.
      iv. *Compute the new hybrid moments* $U_i^{n+1} = U_i^{p,n+1} + U_i^{E,n+1}$.
   (c) *Perform the relaxation step.*
      i. *In each cell set* $N_i^k = \text{Iround}(\lambda N_i^p)$ *and discard* $N_i^p - N_i^k$ *particles.*
      ii. *Compute the new number of particles in the nonequilibrium regime in each cell,* $N_i^p = N_i^k + M_i^p$, $i = 1, \dots, L$, *with* M_i^p *the transported Maxwellian particles.*
      iii. *Compute the effective value* $\lambda_i^p = (N_i^k + M_i^p)/(\varrho_i^{n+1}\Delta x/m^p)$.
      iv. *Set* $\beta_i = 1 - \lambda_i^p$.
   (d) *Set* $t = t + \Delta t$, $n = n + 1$ *and compute the updated value of* Δt.

   end while.

Remark 1.

- In this simple version of the FSI hybrid method the value of the equilibrium fraction fluctuates in each cell around the constant value $\beta = 1 - \lambda$; thus it depends on $\Delta t/\varepsilon$. We will see how to remove this limitation and make the equilibrium fraction essentially independent on Δt in the optimized version of the FSI scheme. Note that fluctuations are due to the fact that to have

Copyright © by SIAM. Unauthorized reproduction of this article is prohibited.

mass conservation during the relaxation step we compute the effective value λ_i^p and set $\beta_i = 1 - \lambda_i^p$.

- To avoid bias in the algorithm we used a stochastic rounding $\mathrm{Iround}(x)$ of a positive real number x defined as

$$\mathrm{Iround}(x) = \begin{cases} [x] & \text{with probability} \quad [x] + 1 - x, \\ [x] + 1 & \text{with probability} \quad x - [x], \end{cases}$$

where $[x]$ denotes the integer part of x.

- In the fluid limit the numerical method is characterized by the particular solver adopted to compute the solution of the Euler equation. Thus the order of accuracy of the limiting scheme is completely independent from the first order splitting procedure used to solve the kinetic equation. This is an advantage compared to the classical approach based on kinetic schemes which gives limited accuracy in time. Extensions to higher order in the nonfluid regime are not trivial since we are limited to first order accuracy in time by Theorem 4.1.

4.1.1. Matching moments. In order to have a conservative scheme it is desirable that the set of transported equilibrium samples satisfies

$$\mathcal{P}(\mathcal{T}_{\Delta t}(\beta(x,t) M_f^p(x,v,t))) = U^E(x, t + \Delta t); \tag{4.10}$$

namely, the kinetic particle solution to the fluid equations in one time step should match the direct solution to the limiting fluid equations. Moreover, since the right-hand side is not affected by statistical sampling error, imposing (4.10) will decrease the variance of the samples.

To this end it is natural to use a moment matching approach (see [4], for example). This can be done by simple transformations of the sample points. Given a set of samples $\nu_1, \dots, \nu_J$ with first two moments μ_1 and μ_2 and a better estimate m_1 and m_2 of the same moments, we can apply the transformation [4, 24]

$$\nu_j^* = \frac{\nu_j - \mu_1}{c + m_1}, \qquad c = \sqrt{\frac{\mu_2^2 - \mu_1^2}{m_2 - m_1^2}}, \quad i = 1, \dots, J, \tag{4.11}$$

to get

$$\frac{1}{J} \sum_{j=1}^{J} \nu_j^* = m_1, \qquad \frac{1}{J} \sum_{j=1}^{J} (\nu_j^*)^2 = m_2.$$

Of course, this renormalization of samples is not possible for the mass density, which depends only on the number of samples. In fact, to keep the algorithm simple, we take the weight of each particle m^p to be equal and constant during the simulation, and this implies that we can have only integer multiples of such weights as mass density values in each cell.

However, thanks to the particular structure of the algorithm, we can also perform a matching procedure for the mass using the following trick. After the transport of Maxwellian particles, in order to perform the moment matching of order zero, we need in each cell a number of particles given by

$$M_i^p = \mathrm{Iround}\left(\frac{\lambda \rho^E(x_i, t + \Delta t)}{m^p} \right).$$

Copyright © by SIAM. Unauthorized reproduction of this article is prohibited.

This can be done if we take $\bar{\lambda}$ large enough before transport to guarantee that we have enough particles in each cell after transport. In this way the difference between the particle mass and the Euler mass is maintained below the mass of one single particle.

Next, to have exact mass conservation we correct λ_i^p and β^p, computing the effective values

$$\lambda_i^p = \frac{(M_i^p + N_i^k)}{\rho^E(x_i, t+\Delta t)\Delta x/m^p + N_i^p}, \quad \beta^p(x_i, t+\Delta t) = 1 - \lambda_i^p,$$

used in the method. After this we renormalize the transported equilibrium samples in each space cell using (4.11), so that they have the same momentum and energy as the Euler solution.

Similarly one can apply a moment matching strategy when sampling from the Maxwellian during the relaxation step. In this case, as an alternative to the moment matching technique described above, one can use the algorithm developed by Pullin [31].

Note that the whole method can be seen as a Monte Carlo scheme for the BGK equation in which we try to reduce fluctuations by substituting the moments of the transported Maxwellian, computed with particles, with the moments given by the solution of the compressible Euler equation, obtained with a deterministic macroscopic scheme. Moreover, as described above, if we force the equilibrium particles to follow the moments given by the fluid equations, we can reinterpret the algorithm as a fluid-dynamic guided Monte Carlo scheme.

4.2. Optimal FSI methods. The method just described does not take into account the possibility of optimizing the equilibrium fraction by increasing its value in time and making it independent of the choice of the time step. In fact at each time step the equilibrium structure is entirely lost, and the new fraction of equilibrium is given by the relaxation step (see (4.8)). However, in principle, it is possible to recover some information from the transported local Maxwellian even if we know it only through samples and not through a deterministic method. We recall, in fact, that we do not get any microscopic information from $U^E(x,t)$, which corresponds to the solution of the Euler equation with a macroscopic numerical scheme. In what follows, we will propose a method for optimizing the equilibrium fraction $\beta(x,t)$ after the transport step. We start describing the generalization of the hybrid method once this optimization has been achieved.

Thanks to Definition 3.1, we can define the velocity dependent optimal equilibrium fraction as the ratio of the transported Maxwellian at time t to the new local Maxwellian at time $n+1$,

$$w^c(x,v,t+\Delta t) = \begin{cases} \dfrac{\mathcal{T}_{\Delta t}(\beta(x,t)M_f(x,v,t))}{M_f^H(x,v,t+\Delta t)}, & \mathcal{T}_{\Delta t}(\beta(x,t)M_f(x,v,t)) \le M_f^H(x,v,t+\Delta t), \\ 1, & \mathcal{T}_{\Delta t}(\beta(x,t)M_f(x,v,t)) \ge M_f^H(x,v,t+\Delta t), \end{cases}$$

and the optimal equilibrium fraction as

$$\beta^c(x,t+\Delta t) = \min_v \{w^c(x,v,t+\Delta t)\}. \tag{4.12}$$

This value can be considered optimal, in the sense that it is the maximum allowed value for which we have a decomposition like

$$\mathcal{T}_{\Delta t}(\beta(x,t)M_f(x,v,t)) = \tilde{M}_f(x,v,t+\Delta t) + \beta^c(x,t+\Delta t)M_f^H(x,v,t+\Delta t) \tag{4.13}$$

Copyright © by SIAM. Unauthorized reproduction of this article is prohibited.

with $\tilde{M}_f(x,v,t+\Delta t) \geq 0$.

Suppose, for simplicity, that $\beta^c(x,t) = 0$ at the beginning of our computation; it follows that the method reads in the same way from (4.4) to (4.7). Now, given an estimation for $\beta^c(x,t+\Delta t)$, the next relaxation step reads as

$$\begin{aligned}\mathcal{R}_{\Delta t}(\mathcal{T}_{\Delta t}(f(x,v,t))) &= \lambda \mathcal{T}_{\Delta t}(f(x,v,t)) + (1-\lambda) M_f^H(x,v,t+\Delta t) \\ &= \lambda(\mathcal{T}_{\Delta t}((1-\beta(x,t))f^p(x,v,t)) + \mathcal{T}_{\Delta t}(\beta(x,t)M_f(x,v,t))) \\ &\quad + (1-\lambda) M_f^H(x,v,t+\Delta t) \\ &= \lambda(\mathcal{T}_{\Delta t}((1-\beta(x,t))f^p(x,v,t)) + \beta^c(x,t+\Delta t) M_f^H(x,v,t+\Delta t) \\ &\quad + \tilde{M}_f(x,v,t+\Delta t)) + (1-\lambda) M_f^H(x,v,t+\Delta t) \\ &= (1-\beta(x,t+\Delta t)) f^p(x,v,t+\Delta t) + \beta(x,t+\Delta t) M_f^H(x,v,t+\Delta t),\end{aligned}$$

with

$$\beta(x,t+\Delta t) = 1 - \lambda(1-\beta^c(x,t+\Delta t)) \tag{4.14}$$

and

$$f^p(x,v,t+\Delta t) = \frac{\mathcal{T}_{\Delta t}((1-\beta(x,t))f^p(x,v,t)) + \tilde{M}_f(x,v,t+\Delta t)}{1-\beta^c(x,t+\Delta t)}. \tag{4.15}$$

In order to sample from the distribution $\tilde{M}_f(x,v,t+\Delta t)$, which is obtained as a difference of two distribution functions (see (4.13)), we can sample particles, exactly as in the previous section, from the transported Maxwellian and then apply the following acceptance-rejection technique.

Algorithm 2 (acceptance-rejection sampling).

1. *Select randomly one particle from the distribution* $\mathcal{T}_{\Delta t}(\beta(x,t)M_f(x,v,t))$.
2. *With probability* $1 - \frac{\beta^c(x,t+\Delta t)M_f^H(x,v,t+\Delta t)}{\mathcal{T}_{\Delta t}(\beta(x,t)M_f(x,v,t))}$ *keep the particle; otherwise discard it.*

In the above algorithm, particles can be chosen more than once; in other words, the sampling is not exclusive. Finally, a moment matching strategy similar to the one described in the previous section can be used in such a way that the equation

$$\mathcal{P}(\tilde{M}_f(x,v,t+\Delta t)) = U^E(x,t+\Delta t) - \beta^c(x,t+\Delta t)\tilde{U}^H(x,t+\Delta t) \tag{4.16}$$

is satisfied exactly.

The major problem we have to face when evaluating $\beta^c(x,t+\Delta t)$ is that $M_f^H(x,v,t+\Delta t)$ is known analytically, while $\mathcal{T}_{\Delta t}(\beta(x,t)M_f(x,v,t))$ is known only through samples. From a numerical viewpoint, when approximating $\beta^c(x,t+\Delta t)$ we want to avoid overestimates since these may produce unphysical solutions. In the following description, to simplify notation, we restrict ourselves to one dimension in velocity and physical space; extensions of the methods to multidimensional cases are straightforward. Our goal is to find a lower estimate of $\beta^c(x,t)$ given by (4.12). Without loss of generality we assume that at each point x there exists a velocity v such that

$$\mathcal{T}_{\Delta t}(\beta(x,t)M_f(x,v,t)) \leq M_f^H(x,v,t+\Delta t).$$

In fact, for those space points x where the above assumption is not satisfied, we simply have $\beta^c(x,t+\Delta t) = 1$.

Copyright © by SIAM. Unauthorized reproduction of this article is prohibited.

The first and simplest method consists of measuring the departure from equilibrium by reconstructing the transported Maxwellian from samples. In order to do that we need a grid in velocity space and a loop over the particles inside each spatial cell. We omit here the details of the different reconstruction methods that can be used; we refer to [27] (and the references therein) for the technical aspects.

Once we have reconstructed $\mathcal{T}_{\Delta t}(\beta(x_i,t)M_f(x_i,v,t))$, with $\{x_i\}_{i\in I}$ a mesh of the physical space, we can evaluate

$$\beta^c(x_i,t+\Delta t)=\min_v\left\{\frac{\mathcal{T}_{\Delta t}(\beta(x_i,t)M_f(x_i,v,t))}{M_f^H(x_i,v,t+\Delta t)}\right\}. \tag{4.17}$$

This method presents several drawbacks. The reconstruction of the distribution function from samples increases the computational cost; moreover, a small number of particles inside a cell, which is quite common in applications, gives large fluctuations, and this results in an imprecise estimate of $\beta^c(x,t)$.

A better way to estimate the equilibrium fraction $\beta^c(x,t)$ after the transport is based on the analysis of a deterministic transport of the Maxwellian part. Again we introduce a grid in space. We consider the following scheme for the transport of the Maxwellian fraction:

$$\begin{aligned}
&\frac{\hat{M}_{f,i}^{n+1}(v)-M_{f,i}^n(v)}{\Delta t}+v\frac{M_{f,i}^n(v)-M_{f,i-1}^n(v)}{\Delta x}=0, \quad v\geq 0,\\
&\frac{\hat{M}_{f,i}(v)^{n+1}-M_{f,i}^n(v)}{\Delta t}+v\frac{M_{f,i+1}^n(v)-M_{f,i}^n(v)}{\Delta x}=0, \quad v<0,
\end{aligned} \tag{4.18}$$

where $M_{f,i}^n(v)\approx M_f(x_i,v,t^n)$, $\hat{M}_{f,i}^{n+1}(v)\approx M_f(x_i,v,t^{n+1})$, and Δx is the mesh size in space. We use the hat notation on the transported Maxwellian to distinguish it from the local Maxwellian at time $t+\Delta t$, which, according to our notation, is $M_{f,i}^{n+1}(v)$. The scheme described above is a simple first order upwind for the Maxwellian transport. Of course to effectively perform the computation it is necessary to truncate the Maxwellian in order to obtain finite values for the velocity and a time step larger than zero. Typically this truncation leads to several problems which are common in numerical methods for kinetic equations (see, for example, [19, 26]). Here we are interested only in estimating the departure from the equilibrium of the transported Maxwellian, and for this aim we choose a bound for the velocity space in such a way that no additional time step restrictions for the whole scheme are imposed. Solving (4.18), we obtain

$$\begin{aligned}
\hat{M}_{f,i}^{n+1}(v)&=\left(1-\frac{v\Delta t}{\Delta x}\right)M_{f,i}^n(v)+\frac{v\Delta t}{\Delta x}M_{f,i-1}^n(v), \quad v\geq 0,\\
\hat{M}_{f,i}^{n+1}(v)&=\left(1+\frac{v\Delta t}{\Delta x}\right)M_{f,i}^n(v)-\frac{v\Delta t}{\Delta x}M_{f,i+1}^n(v), \quad v<0.
\end{aligned} \tag{4.19}$$

Note that, since $|v|\Delta t\leq\Delta x$, the updated function $\hat{M}_{f,i}^{n+1}(v)$ is a convex combination of the local Maxwellian in the cells i and $i-1$ for positive velocities, and in the cells i and $i+1$ for negative velocities.

Now, ignoring the error introduced by the truncation in velocity, in each cell the equilibrium fraction $\beta^c(x_i,t+\Delta t)$ satisfies

$$\beta^c(x_i,t+\Delta t)=\min_v\left\{\frac{\mathcal{T}_{\Delta t}(\beta(x_i,t)M_f(x_i,v,t))}{M_f^H(x_i,v,t+\Delta t)}\right\}=\min_v\left\{\frac{\hat{M}_{f,i}^{n+1}(v)}{M_{f,i}^{H,n+1}(v)}\right\}+O(\Delta t^2). \tag{4.20}$$

Copyright © by SIAM. Unauthorized reproduction of this article is prohibited.

In the general case a numerical method is required to compute the minimum on the right-hand side. This operation can be expensive since it has to be done at each time step and in each spatial cell. However, we can restrict ourselves to a lower estimate of $\beta^c(x_i, t+\Delta t)$ (to avoid an overestimate of the equilibrium fraction), and instead of the minimum we can choose a lower bound for (4.20) using the convexity property of the scheme. That value can be estimated by observing that

$$\min_{v\geq 0}\left\{\frac{\hat{M}^{n+1}_{f,i}(v)}{M^{H,n+1}_{f,i}(v)}\right\} \geq \min\left\{\min_{v\geq 0}\left\{\frac{M^{n}_{f,i}(v)}{M^{H,n+1}_{f,i}(v)}\right\}, \min_{v\geq 0}\left\{\frac{M^{n}_{f,i-1}(v)}{M^{H,n+1}_{f,i}(v)}\right\}\right\}$$
$$= \beta^c_R(x, t+\Delta t), \tag{4.21}$$

$$\min_{v<0}\left\{\frac{\hat{M}^{n+1}_{f,i}(v)}{M^{H,n+1}_{f,i}(v)}\right\} \geq \min\left\{\min_{v<0}\left\{\frac{M^{n}_{f,i}(v)}{M^{H,n+1}_{f,i}(v)}\right\}, \min_{v<0}\left\{\frac{M^{n}_{f,i+1}(v)}{M^{H,n+1}_{f,i}(v)}\right\}\right\}$$
$$= \beta^c_L(x, t+\Delta t), \tag{4.22}$$

and setting

$$\beta^c(x, t+\Delta t) = \min\{\beta^c_R(x, t+\Delta t), \beta^c_L(x, t+\Delta t)\}, \tag{4.23}$$

where the minimum of the ratios in (4.21)–(4.22) can be computed exactly, being the ratios of Maxwellian functions.

An algorithm that can be used to implement the optimized FSI method for the solution of the BGK equation, in which for simplicity λ is constant, is the following.

ALGORITHM 3 (optimized FSI hybrid scheme).

1. *Compute the initial velocity and position of the particles* $\{\nu^0_j, j=1,\dots,N\}$, $\{p^0_j, j=1,\dots,N\}$ *by sampling them from initial density* $f_0(x,v)$. *Set* $m^p = \int\int f_0(x,v)dxdv/N$.
2. *Given a mesh* x_i, $i=1,\dots,L$, *with grid size* Δx, *and an estimate of the larger sample velocity* $\nu_{max} = 4\sqrt{2T_{max}}$, *with* T_{max} *the maximum temperature, set* $\Delta t^p = \Delta x/\nu_{max}$.
3. *Compute the initial values of the moments of the distribution function in each cell* ϱ_i, $(\varrho u)_i$, E_i, $i=1,\dots,L$.
4. *Compute the larger time step allowed by the deterministic macroscopic scheme* Δt_D.
5. *Set* $\Delta t = \min(\Delta t^p, \Delta t_D)$.
6. *Set* $n=0$, $t=0$, $\lambda = e^{-\Delta t/\varepsilon}$, $\bar{\lambda}=\lambda$, $\beta_i = 1-\bar{\lambda}$, $i=1,\dots,L$.
7. *While* $t \leq t_f$ *with* t_f *the final chosen time, do the following:*
   (a) *Estimate the number of Maxwellian samples that we need from* $\bar{\lambda}\beta(x,t)M^p_f(x,v,t)$.
      i. *In each cell set* $N^M_i = \mathrm{Iround}(\beta_i\rho^n_i/(m^p/\Delta x))$, *and sample* N^M_i *equilibrium particles from the Maxwellian with moments* $(\rho u)^n_i, E^n_i$.
   (b) *Perform the transport step, keeping track of the particles that come from the above sampling.*
      i. *Transport all particles*

$$p^{n+1}_j = p^n_j + \nu^n_j\Delta t \quad \forall\, j. \tag{4.24}$$

      ii. *Compute the moments* $U^{p,n+1}_i$ *and the number of particles* N^p_i *in each cell using only the advected particles not sampled from the Maxwellian.*

Copyright © by SIAM. Unauthorized reproduction of this article is prohibited.

iii. *Solve the Euler equations for* $U_i^{E,n} = \beta_i U_i^n$ *and find* $U_i^{E,n+1}$.
iv. *Compute the new hybrid moments* $U_i^{n+1} = U_i^{p,n+1} + U_i^{E,n+1}$.

(c) *Compute the optimal equilibrium fraction* $\beta_i^{c,n+1}$ *as described in* (4.21)–(4.23).

(d) *Perform the relaxation step.*
i. *In each cell set* $N_i^k = \mathrm{Iround}(\lambda N_i^p)$ *and discard* $N_i^p - N_i^k$ *particles.*
ii. *In each cell sample* $\tilde{N}_i^M$ *particles from the distribution* $\tilde{M}_{f,i}^{n+1}(v)$ *with the acceptance-rejection technique described in Algorithm* 2.
iii. *Apply the moment matching technique to the* $\tilde{N}_i^M$ *particles in order to satisfy* (4.16).
iv. *Compute the new number of particles in the nonequilibrium regime in each cell,* $N_i^p = N_i^k + \tilde{N}_i^M$, $i = 1, \ldots, L$.
v. *Compute the effective equilibrium fraction, which is* $\beta_i = 1 - (N_i^k + \tilde{N}_i^M)/(\varrho_i^{n+1} \Delta x / m^p)$.

(e) *Set* $t = t + \Delta t$, $n = n + 1$ *and compute the updated value of* Δt.

end while.

Remark 2.

- We emphasize that the first order upwind method for computing the deterministic transport of Maxwellians is never used in practice. It serves us only as an approximation strategy in order to compute a lower bound for the optimal equilibrium fraction $\beta^c(x, t + \Delta t)$. In this sense it is worth noticing that the additional first order dissipation introduced by this upwinding produces additional smearing and in principle, close to discontinuities, can produce overestimates of the equilibrium fraction when computed from (4.20). Besides computational efficiency, this is an additional motivation for using a lower bound for that value.
- The hybrid composition of the solution in the final method does not depend on the time step Δt but only on ε. Note, however, that small time steps, below the CFL condition of the deterministic Euler solver, may increase the computational cost. To reduce this effect one can use different time steps in the kinetic and the Euler solvers and perform the hybridization and matching only at intermediate steps. This strategy can be used, for example, where there is the need to resolve small scales at the Navier–Stokes level or in boundary layer effects.

5. Implementation and numerical tests. In principle any finite volume or finite difference numerical scheme can be used to solve the compressible Euler equations in our hybrid method. In what follows we will use a second order finite volume MUSCL-type relaxed scheme (see [18] for details).

In the next sections we analyze the performances of the FSI hybrid schemes in comparison with a classical Monte Carlo method (MCM) for several one-dimensional problems with different Knudsen numbers ranging from $\varepsilon = 10^{-2}$ to $\varepsilon = 10^{-5}$.

As a reference solution we use a deterministic discrete velocity model (DVM) for the BGK equation for all tests (see [19] for details). We use the shorthand FSI, FSI1, and TVD to denote the simple FSI method, the optimal FSI method, and the second order in space MUSCL Euler solver, respectively.

5.1. Accuracy test. Because our aim is to compare the differences in accuracy and computational time between the different methods, first we consider an accuracy test with a periodic smooth solution. We compare the results of the kinetic solver–based hybrid methods developed in [13] with those of the new FSI schemes.

Copyright © by SIAM. Unauthorized reproduction of this article is prohibited.

TABLE 5.1

Accuracy test. Computational times for FSI and FSI1, with two different initial numbers of particles $N = 1500$ and $N_1 = 500$, compared to the previous hybrid methods (see [13]) for different values of the Knudsen number.

	$\varepsilon = 10^{-2}$	$\varepsilon = 10^{-3}$	$\varepsilon = 10^{-4}$	$\varepsilon = 10^{-5}$
MCM N=1500	23 sec	25 sec	27 sec	26 sec
BHM N=1500	35 sec	25 sec	22 sec	22 sec
BHM1 N=1500	34 sec	20 sec	19 sec	20 sec
BCHM N=1500	15 sec	11 sec	17 sec	21 sec
FSI N=1500	25 sec	22 sec	3 sec	0.6 sec
FSI1 N=1500	18 sec	17 sec	2 sec	0.6 sec
FSI N=500	9 sec	8 sec	0.4 sec	0.3 sec
FSI1 N=500	7 sec	6 sec	0.4 sec	0.3 sec

We report the total L^1-norm of the errors for the conserved quantities ϱ, u, T and the corresponding computational times for a problem with the following initial data:

$$\begin{aligned} \varrho(x,0) &= 1 + a_\varrho \sin\frac{2\pi x}{L}, \\ u(x,0) &= 1.5 + a_u \sin\frac{2\pi x}{L}, \\ E(x,0) &= 2.5 + a_T \sin\frac{2\pi x}{L}, \end{aligned} \tag{5.1}$$

where we set

$$a_\varrho = 0.3, \quad a_u = 0.1, \quad a_E = 1.$$

The equations are integrated for $t \in [0, 5 \times 10^{-2}]$ using a 200 space cell.

In order to make a fair comparison with the previous schemes, named BHM, BHM1, and BCHM (see [13] for details and parameter settings of the methods), we use at the beginning 1500 particles for cell with the same time step of the Boltzmann-BGK schemes. Then, because in general FSI-type schemes allow larger time steps and because the moment matching techniques produce lower fluctuations, we repeat the computation with $N = 500$ and the time step prescribed by the MCM. We note that, while estimating the time differences between the FSI schemes and MCM is quite easy (in fact, the FSI methods are based on the MCM for the kinetic part), the same comparison with another kinetic solver, such as DVM or BHM, is not straightforward due to the several possible choices involved in those schemes (for example, the way the velocity domain is truncated and the type of solver chosen for the space derivatives). For this reason we stress that the simulations times, reported in Table 5.1, are just indicative. It is clear that the hybrid methods developed here represent a substantial improvement when compared with the previous schemes as well as with the classical MCM in terms of computational time. In Figure 5.1 we report the total number of particles used by the different algorithms. Note how computational time and fluctuations reduce dramatically when the Knudsen number diminishes.

The results for the relative L^1 errors are reported in Tables 5.2, 5.3, and 5.4, respectively, for density, mean velocity, and temperature for the FSI, FSI1, and Monte Carlo schemes. In all the methods we use $N = 200$ particles for the cell and the moment matching techniques. We notice that the hybrid methods have approximately

Copyright © by SIAM. Unauthorized reproduction of this article is prohibited.

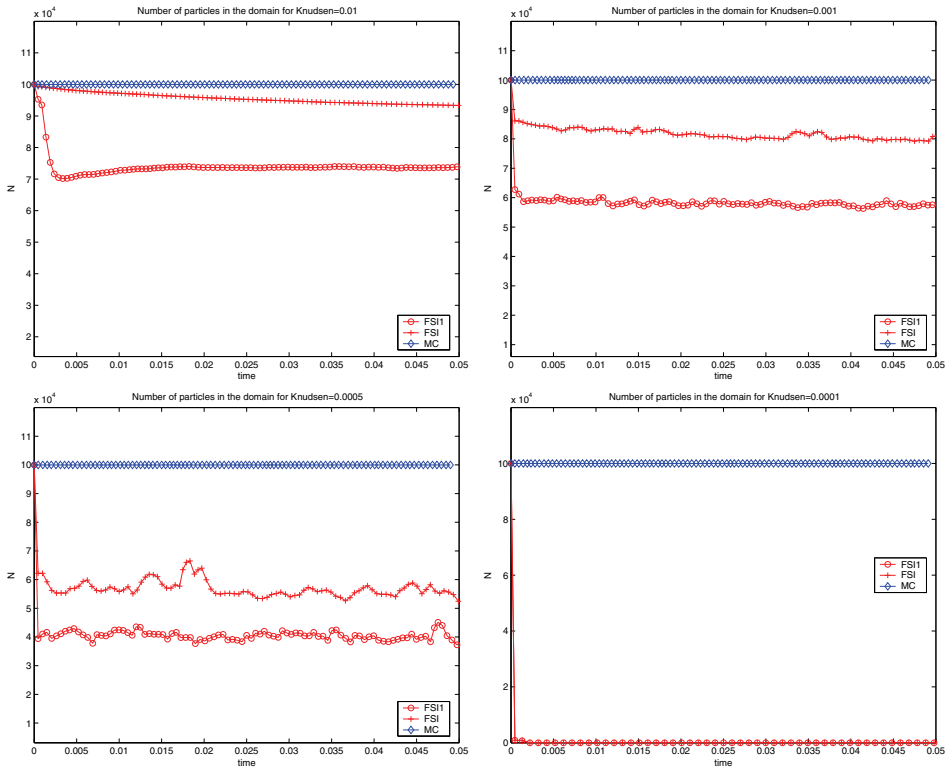

FIG. 5.1. *Accuracy test. Number of particles in time inside the computational domain for FSI1, FSI, and MC schemes. Knudsen numbers* $\varepsilon = 10^{-2}$ *(top left),* $\varepsilon = 10^{-3}$ *(top right),* $\varepsilon = 5 \times 10^{-4}$ *(bottom left), and* $\varepsilon = 10^{-4}$ *(bottom right).*

TABLE 5.2

Accuracy test. L^1*-norm of the error (in units of* 10^{-2}*) for the density with respect to different values of the Knudsen number* ε*.*

	$\varepsilon = 10^{-2}$	$\varepsilon = 10^{-3}$	$\varepsilon = 5 \times 10^{-4}$	$\varepsilon = 10^{-4}$
MCM	5.494	5.786	5.153	5.184
FSI	5.545	3.926	3.067	0.268
FSI1	4.588	3.406	2.451	0.243

the same accuracy as the Euler solver for small Knudsen numbers and the same accuracy as the MCM for large Knudsen numbers, while to intermediate values correspond intermediate behaviors. From the above results it is clear that the performance of the hybrid schemes is better than that of the MCM; moreover, FSI1 gives in general better results than does FSI, both in terms of computational time and accuracy, for almost all regimes.

5.2. 1-D unsteady shock. Next we consider an unsteady shock that propagates from left to right. The shock is produced by miming a specular wall on the left boundary; thus for the stochastic component at each time step, particles which escape from the computational domain on the left side are put back into the first cell with opposite velocity and opposite position with respect to zero. On the other side particles are injected with the initial mean velocity and temperature in a number which

Copyright © by SIAM. Unauthorized reproduction of this article is prohibited.

TABLE 5.3
Accuracy test. L^1-norm of the error (in units of 10^{-2}) for the mean velocity with respect to different values of the Knudsen number ε.

	$\varepsilon = 10^{-2}$	$\varepsilon = 10^{-3}$	$\varepsilon = 5 \times 10^{-4}$	$\varepsilon = 10^{-4}$
MCM	6.565	5.437	5.338	6.035
FSI	4.802	4.401	3.264	0.641
FSI1	5.135	4.102	2.848	0.610

TABLE 5.4
Accuracy test. L^1-norm of the error (in units of 10^{-2}) for the temperature with respect to different values of the Knudsen number ε.

	$\varepsilon = 10^{-2}$	$\varepsilon = 10^{-3}$	$\varepsilon = 5 \times 10^{-4}$	$\varepsilon = 10^{-4}$
MCM	6.762	7.611	7.578	7.316
FSI	7.007	6.022	4.500	0.641
FSI1	6.662	4.939	3.773	0.598

corresponds to the initial density. For the macroscopic part the usual specular and inflow boundary conditions are used. At the beginning the flow is uniform with mass $\varrho = 1$, mean velocity $u = -1$, and energy $E = 2.5$. The computations are stopped when $t = 0.065$, the number of cells is 200 in space, while the initial number of particles is 500 for each space cell. In each figure the solution computed with the Euler scheme and the one computed with the DVM scheme is reported. The FSI, FSI1, and MCM are respectively depicted for density, mean velocity, and temperature. We observe that for large Knudsen numbers FSI (Figure 5.2 left) and FSI1 (Figure 5.2 right) provide a small improvement as compared to MCM (Figure 5.3 left) in terms of fluctuations. When ε decreases, the nonequilibrium part becomes smaller, and both FSI and FSI1 (Figure 5.4 and 5.5) contain fewer fluctuations than does MCM. Note that, since the time step here is $O(\varepsilon)$, the reduction of fluctuations in the FSI scheme is essentially the same for $\varepsilon = 0.001$ and $\varepsilon = 0.0005$, whereas for the FSI1 scheme the solution shows a remarkable improvement as ε diminishes. Finally for $\varepsilon = 10^{-4}$ (Figure 5.6) we are in an underresolved regime, and both hybrid methods yield similar solutions at the same computational time, with strong fluctuation reduction compared to the MCM (Figure 5.7).

5.3. 1-D Lax shock tube test. Finally we consider a Lax shock tube test with initial values

$$\mathbf{u}_L = \begin{pmatrix} 0.445 \\ 0.598 \\ 3.5 \end{pmatrix} \text{ if } 0 \le x < 0.5, \qquad \mathbf{u}_R = \begin{pmatrix} 0.5 \\ 0 \\ 0.48 \end{pmatrix} \text{ if } 0.5 \le x \le 1.$$

The solution is computed with 200 grid points in space; the final time is $t = 0.05$. The initial number of particle is 500 for each space cell. Each figure contains the DVM solution and the Euler solution for reference. Considerations similar to those of the previous section hold for this test case. Thus for large Knudsen numbers the solutions computed with the hybrid methods (Figures 5.8–5.9) show small improvements compared to the MCM (Figures 5.10–5.11). On the other hand, when the Knudsen number becomes smaller, the FSI and FSI1 schemes (Figures 5.12–5.13) give a considerable reduction of fluctuations. This is especially true for the FSI1 method, which demonstrates the importance of a good estimate of the equilibrium fraction β^c after the transport.

Copyright © by SIAM. Unauthorized reproduction of this article is prohibited.

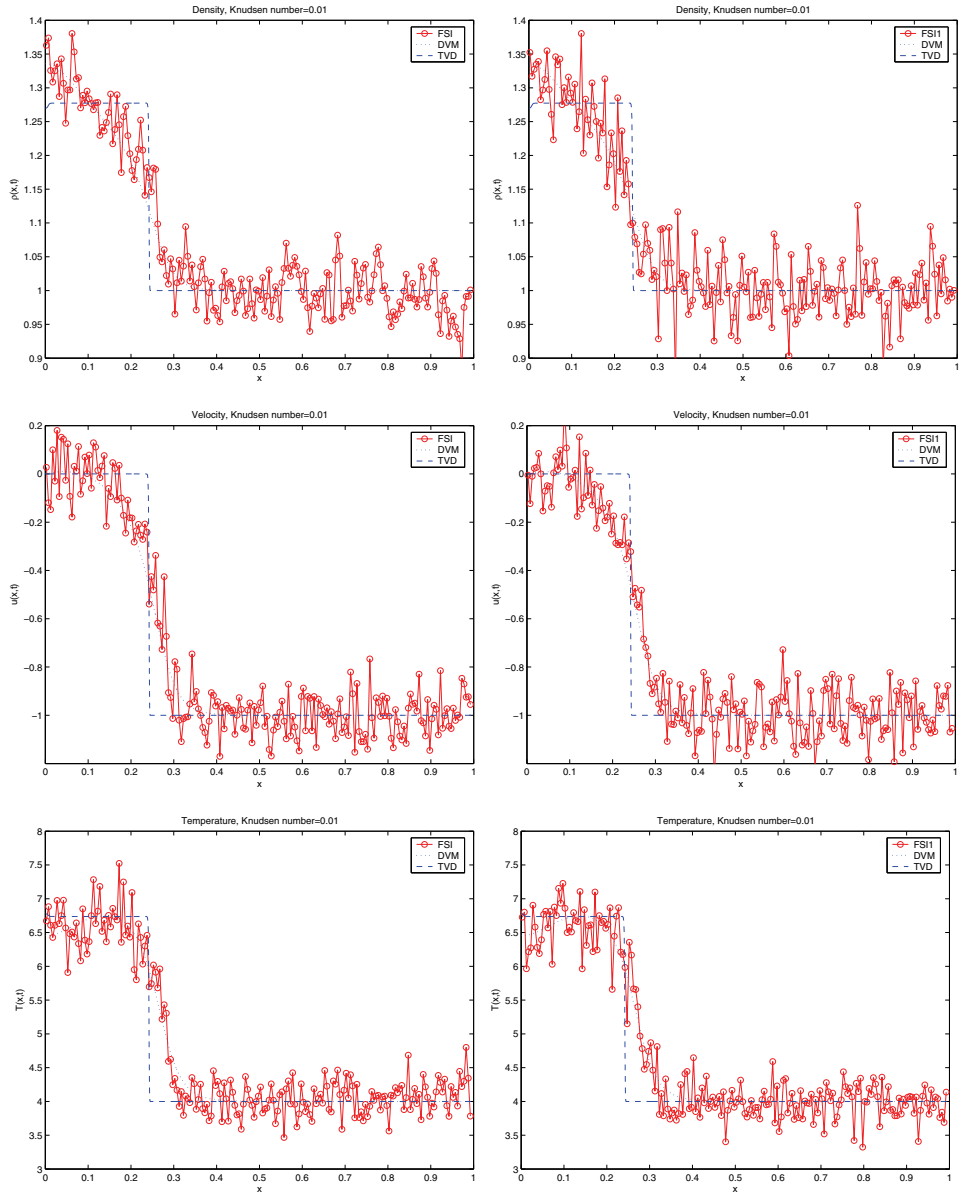

FIG. 5.2. *Unsteady shock:* $\varepsilon = 10^{-2}$. *Solution at* $t = 0.065$ *for FSI (left) and FSI*1 *(right). From top to bottom, density, mean velocity, and temperature.*

Copyright © by SIAM. Unauthorized reproduction of this article is prohibited.

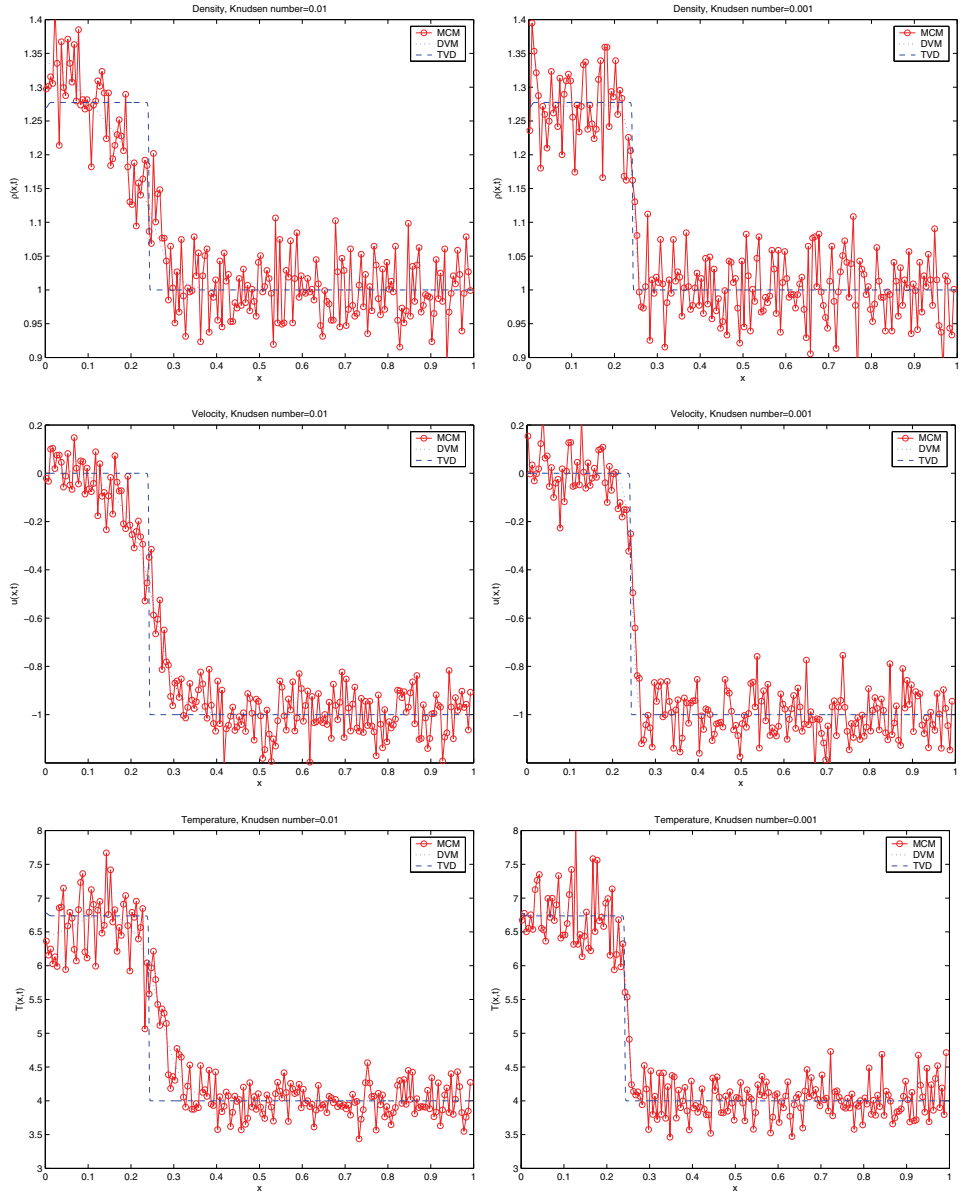

FIG. 5.3. *Unsteady shock. Solution at* $t = 0.065$ *for MCM with Knudsen numbers* $\varepsilon = 10^{-2}$ *(left) and* $\varepsilon = 10^{-3}$ *(right). From top to bottom, density, mean velocity, and temperature.*

Copyright © by SIAM. Unauthorized reproduction of this article is prohibited.

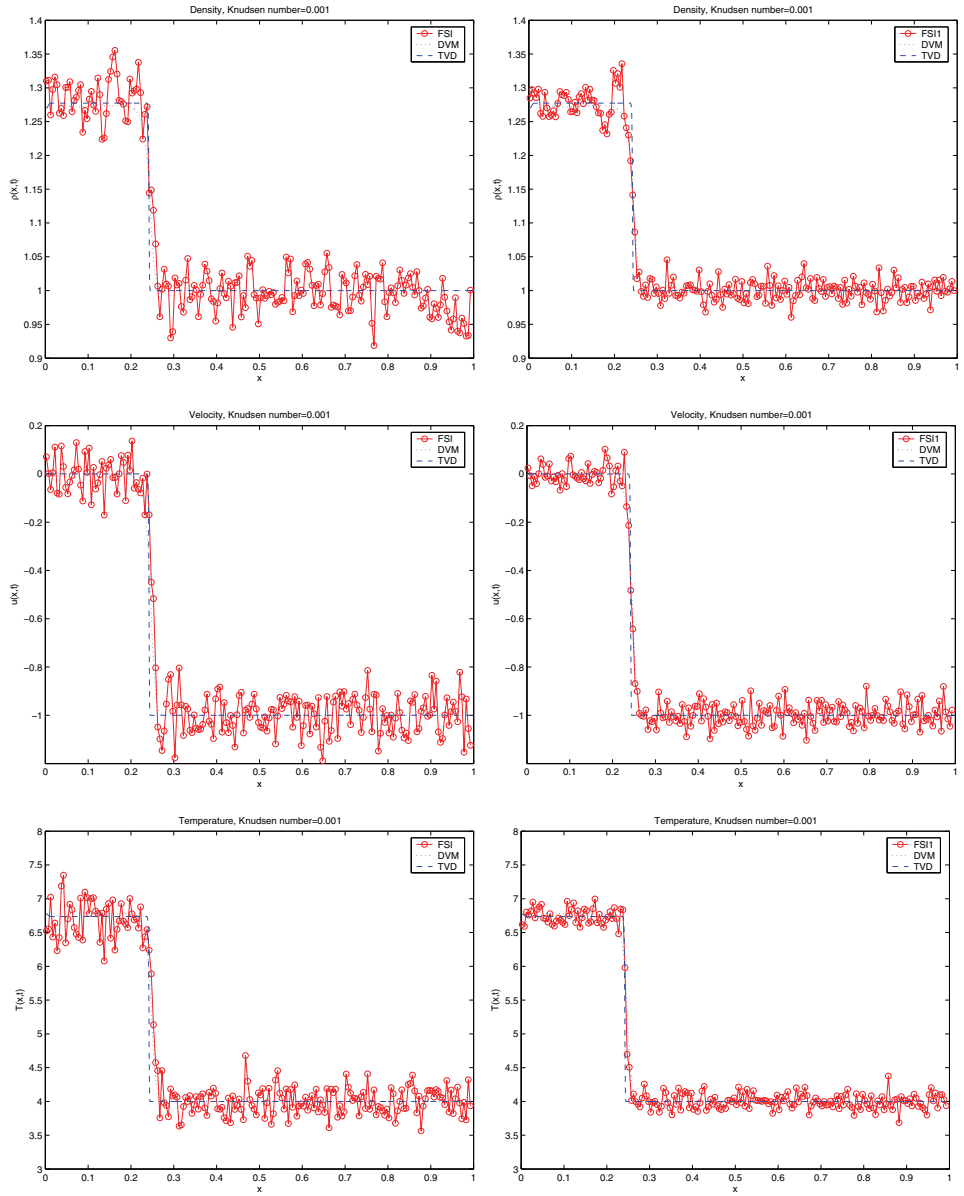

FIG. 5.4. *Unsteady shock:* $\varepsilon = 10^{-3}$. *Solution at* $t = 0.065$ *for FSI (left) and FSI*1 *(right). From top to bottom, density, mean velocity, and temperature.*

Copyright © by SIAM. Unauthorized reproduction of this article is prohibited.

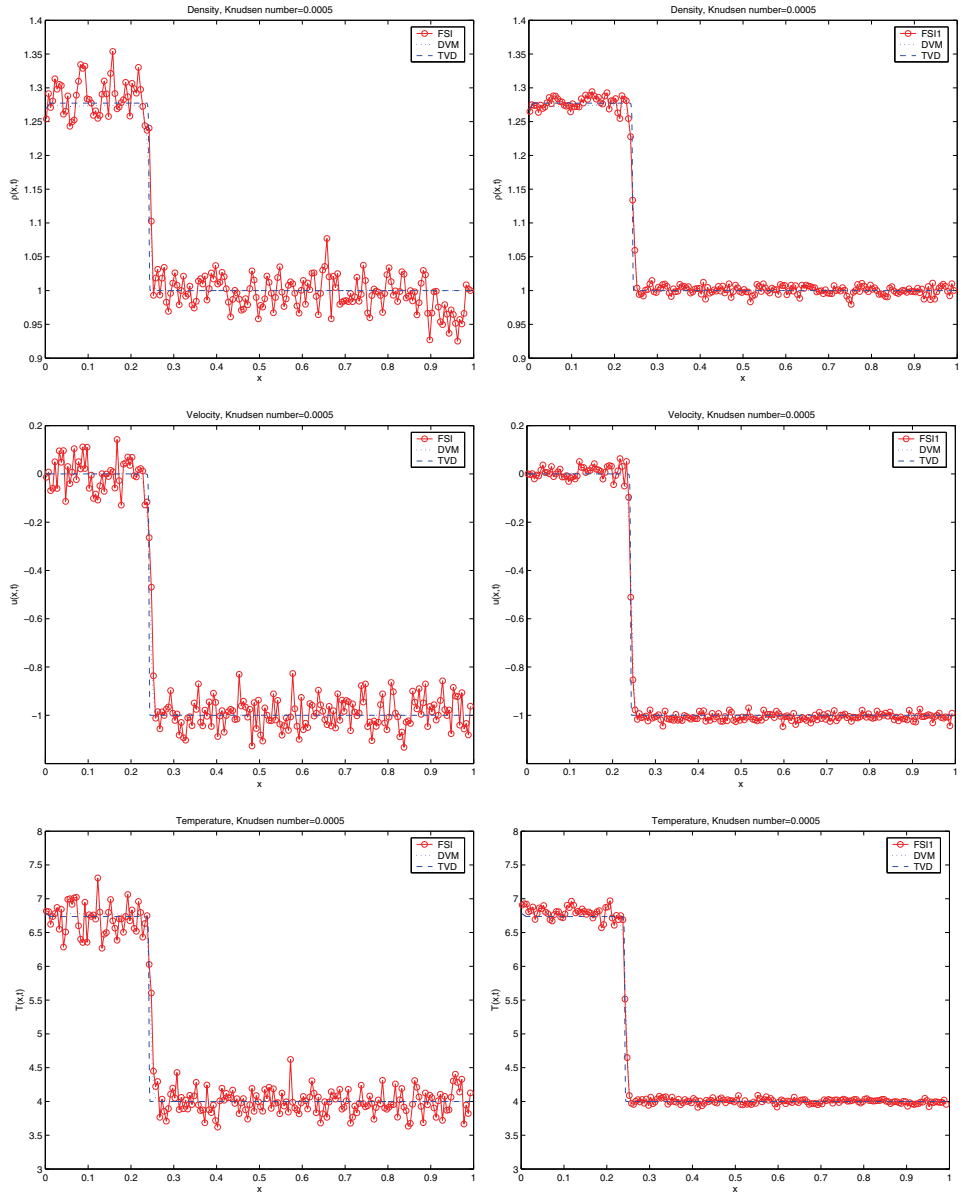

FIG. 5.5. *Unsteady shock:* $\varepsilon = 5 \times 10^{-4}$. *Solution at* $t = 0.065$ *for FSI (left) and FSI*1 *(right). From top to bottom, density, mean velocity, and temperature.*

Copyright © by SIAM. Unauthorized reproduction of this article is prohibited.

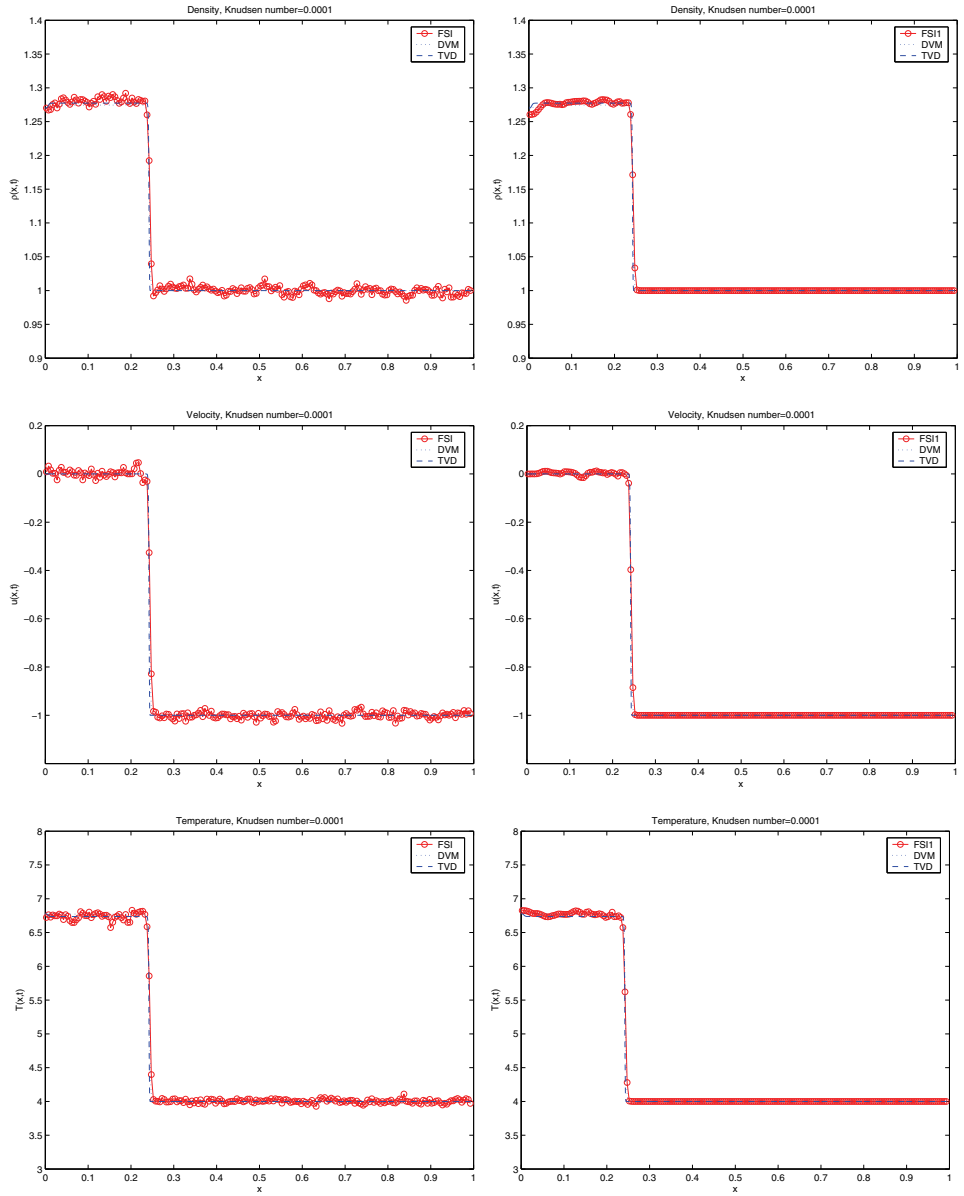

FIG. 5.6. *Unsteady shock:* $\varepsilon = 10^{-4}$. *Solution at* $t = 0.065$ *for FSI (left) and FSI*1 *(right). From top to bottom, density, mean velocity, and temperature.*

Copyright © by SIAM. Unauthorized reproduction of this article is prohibited.

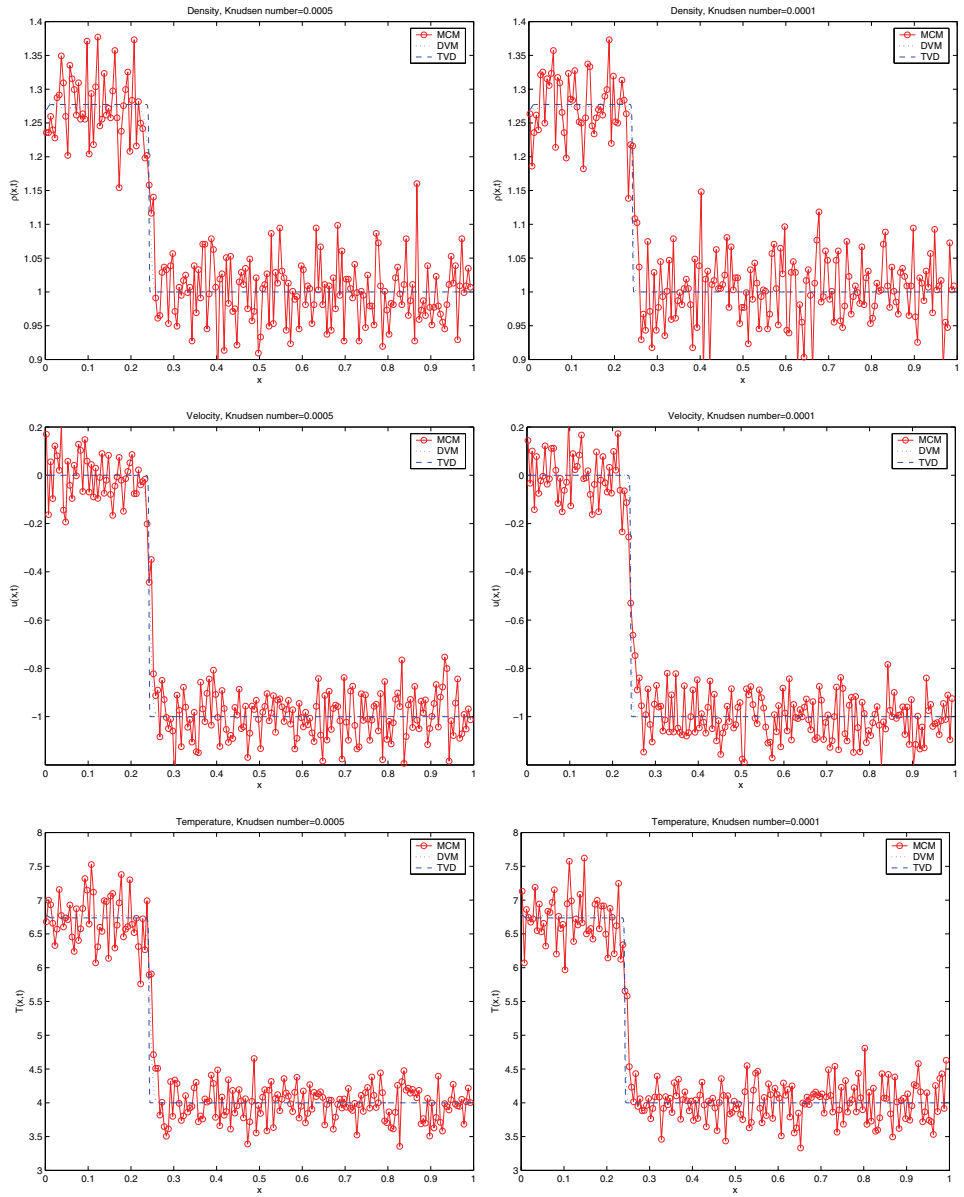

FIG. 5.7. *Unsteady shock. Solution at* $t = 0.065$ *for MCM with Knudsen numbers* $\varepsilon = 5 \times 10^{-4}$ *(left) and* $\varepsilon = 10^{-4}$ *(right). From top to bottom, density, mean velocity, and temperature.*

Copyright © by SIAM. Unauthorized reproduction of this article is prohibited.

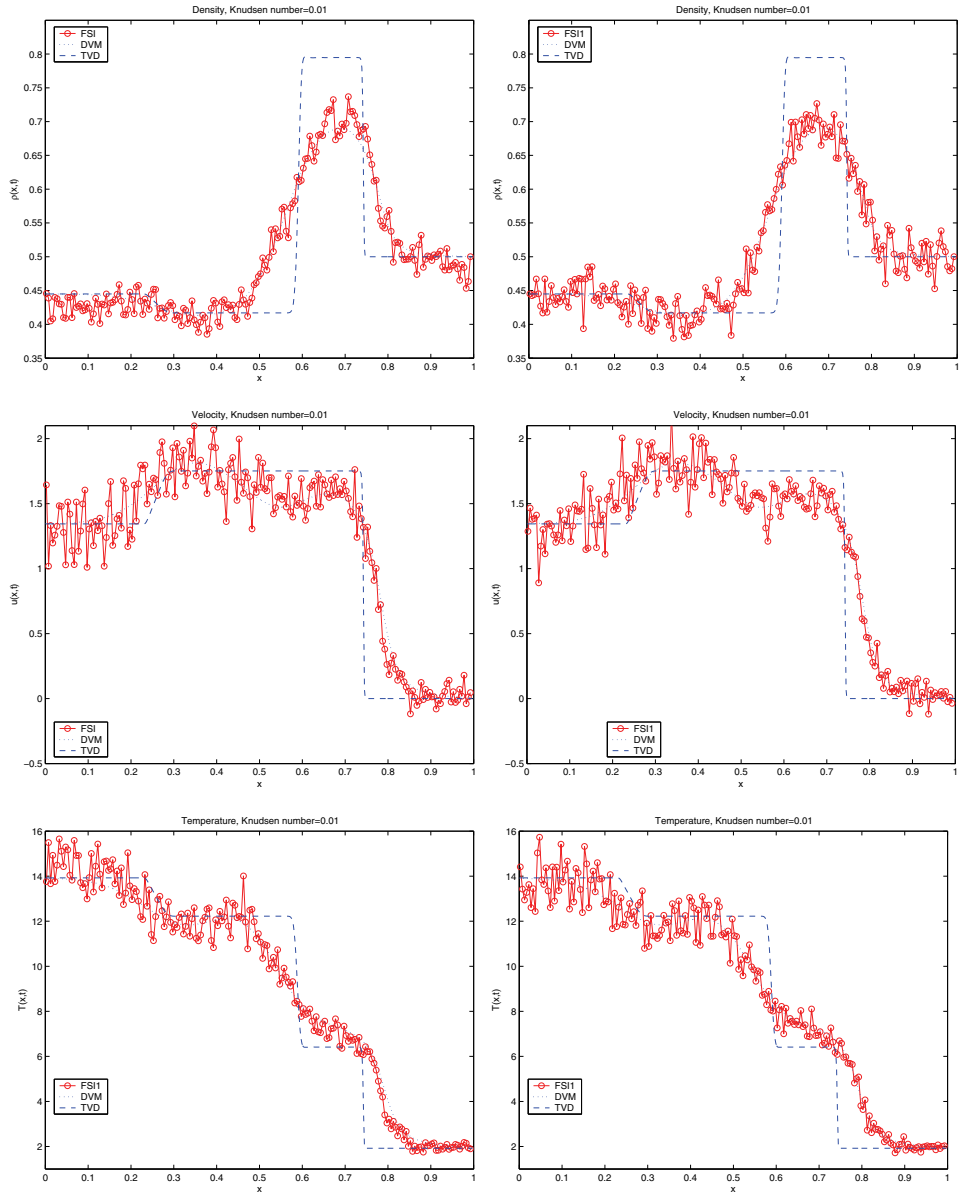

FIG. 5.8. *Lax test:* $\varepsilon = 10^{-2}$. *Solution at* $t = 0.05$ *for FSI (left) and FSI*1 *(right). From top to bottom, density, mean velocity, and temperature.*

Copyright © by SIAM. Unauthorized reproduction of this article is prohibited.

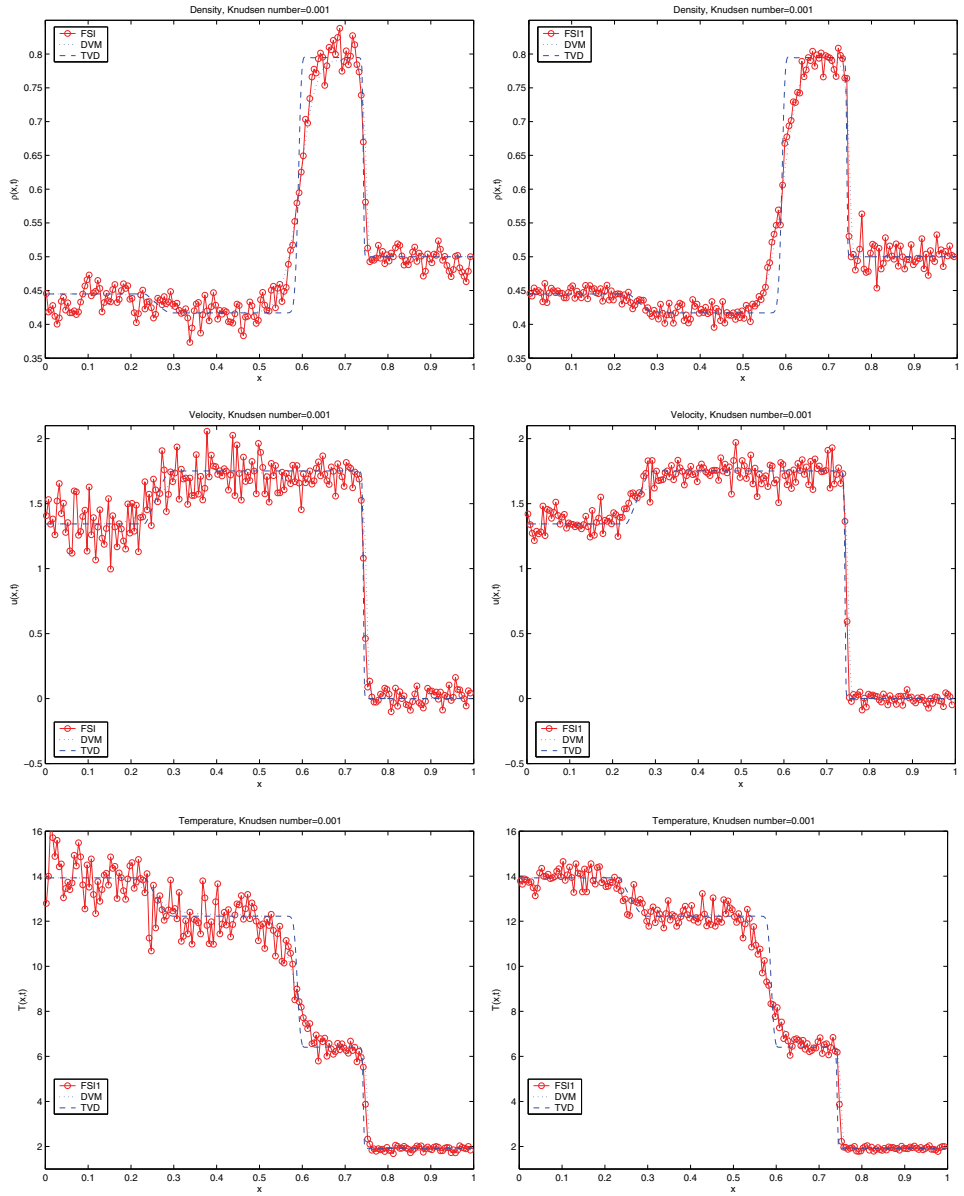

FIG. 5.9. *Lax test:* $\varepsilon = 10^{-3}$. *Solution at* $t = 0.05$ *for FSI (left) and FSI*1 *(right). From top to bottom, density, mean velocity, and temperature.*

Copyright © by SIAM. Unauthorized reproduction of this article is prohibited.

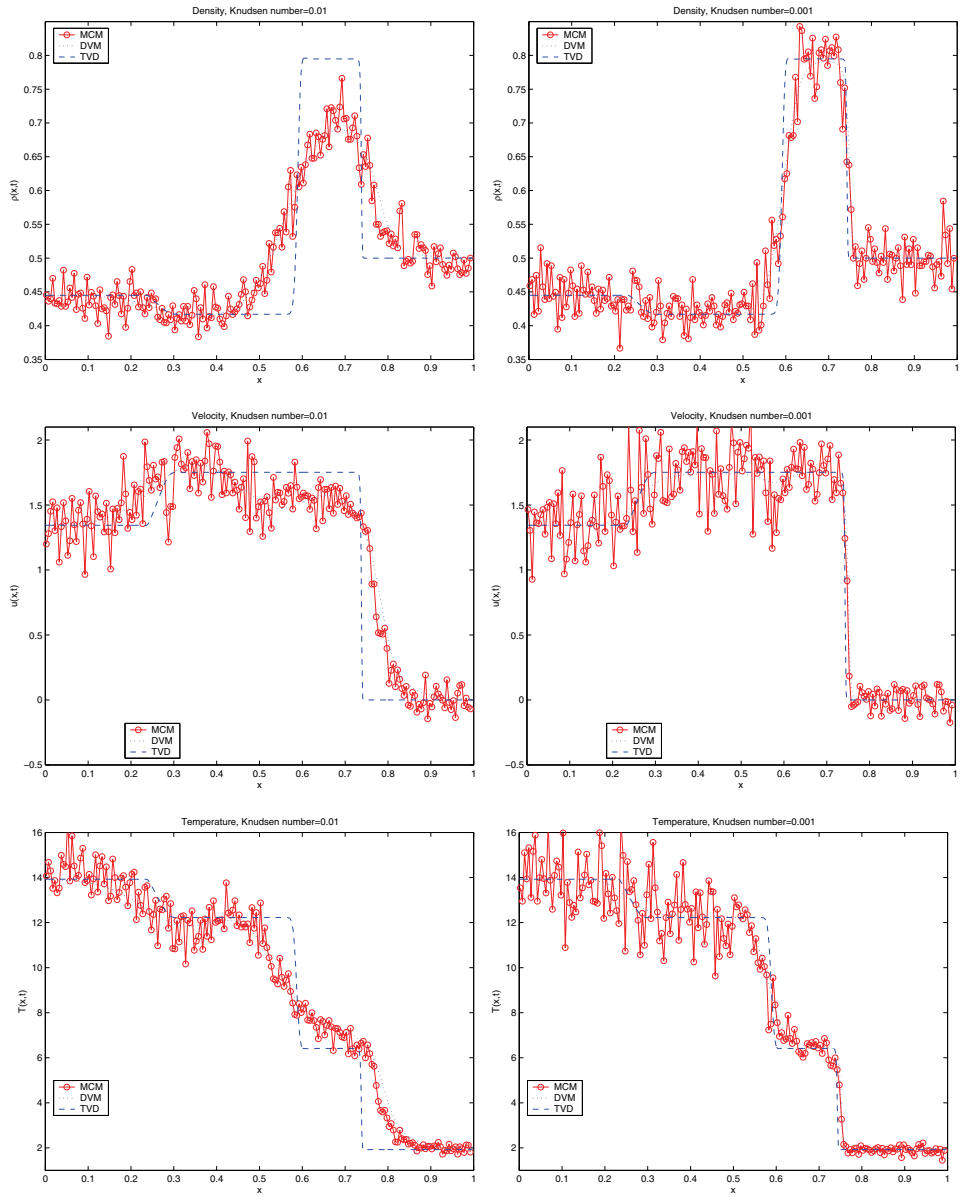

FIG. 5.10. *Lax test. Solution at* $t = 0.05$ *for MCM with Knudsen numbers* $\varepsilon = 5 \times 10^{-2}$ *(left) and* $\varepsilon = 10^{-3}$ *(right). From top to bottom, density, mean velocity, and temperature.*

Copyright © by SIAM. Unauthorized reproduction of this article is prohibited.

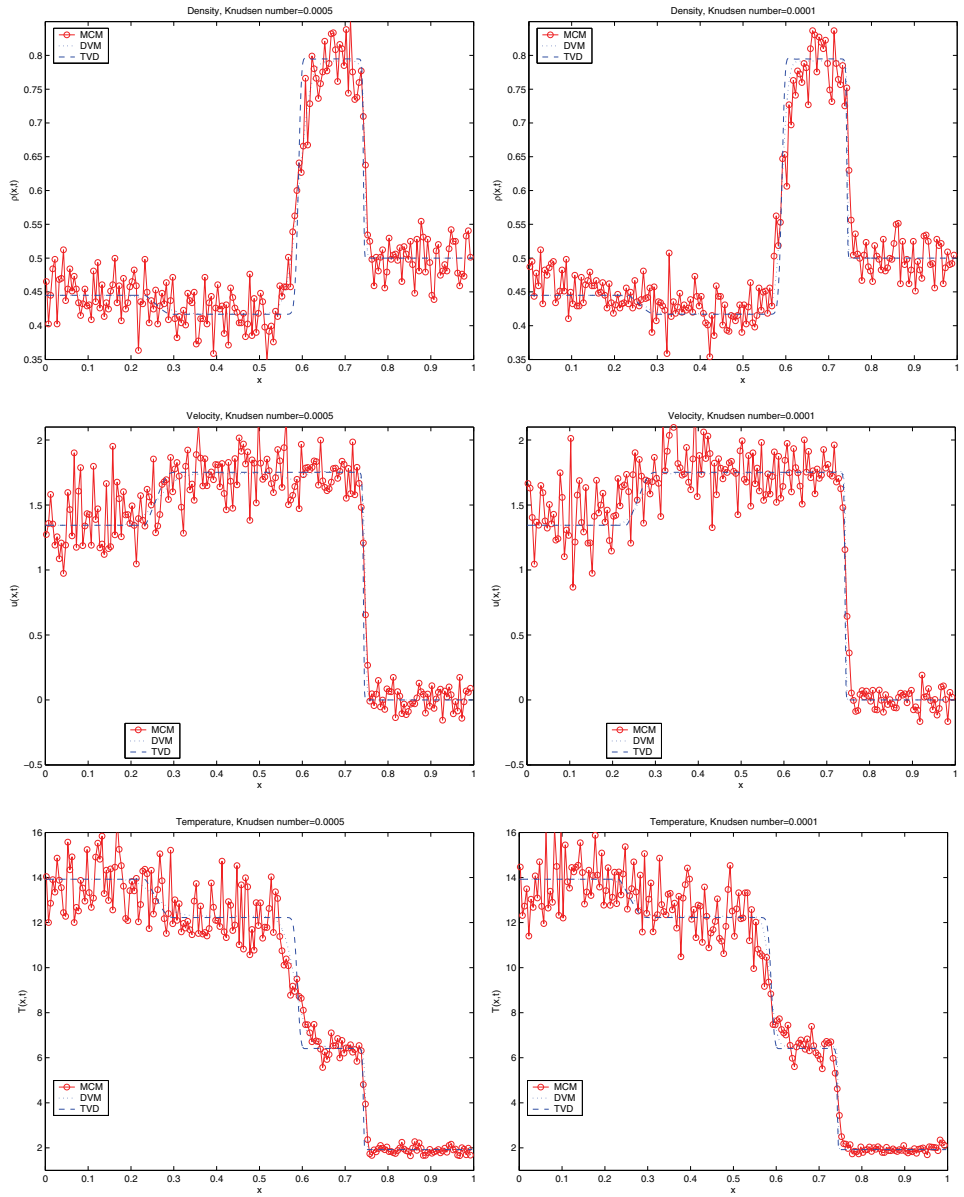

FIG. 5.11. *Lax test. Solution at* $t = 0.05$ *for MCM with Knudsen numbers* $\varepsilon = 5 \times 10^{-4}$ *(left) and* $\varepsilon = 10^{-4}$ *(right). From top to bottom, density, mean velocity, and temperature.*

Copyright © by SIAM. Unauthorized reproduction of this article is prohibited.

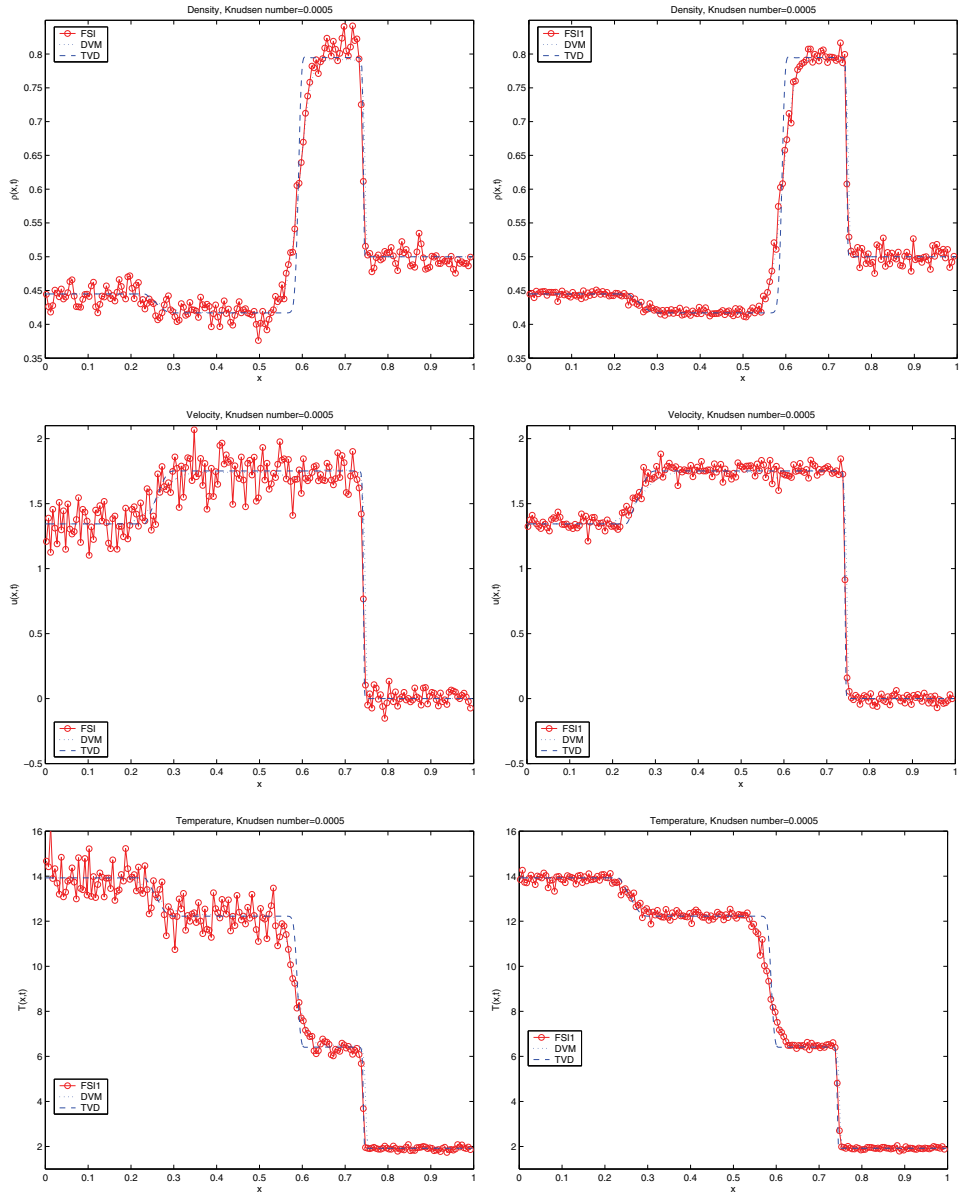

FIG. 5.12. *Lax test:* $\varepsilon = 5 \times 10^{-4}$. *Solution at* $t = 0.05$ *for FSI (left) and FSI*1 *(right). From top to bottom, density, mean velocity, and temperature.*

Copyright © by SIAM. Unauthorized reproduction of this article is prohibited.

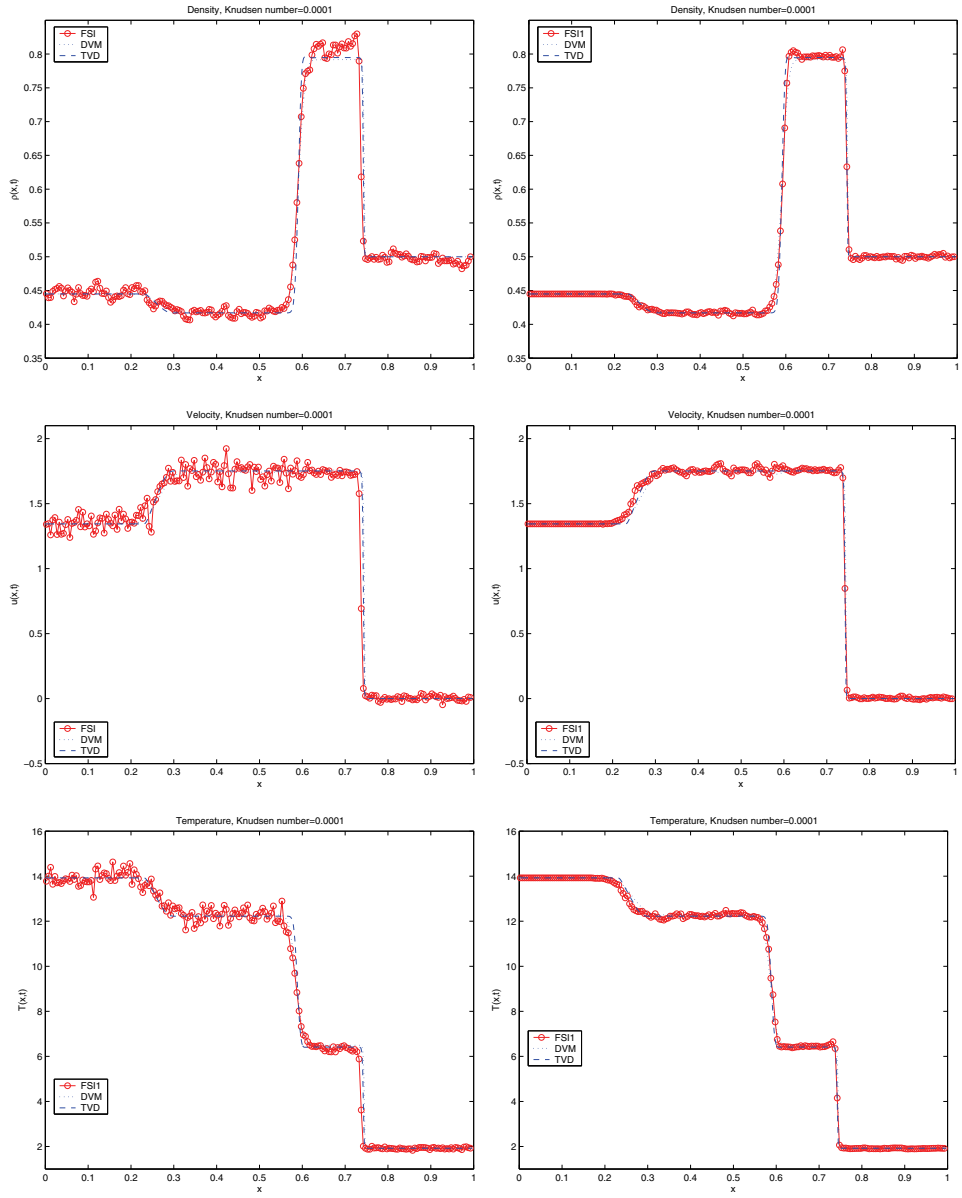

FIG. 5.13. *Lax test:* $\varepsilon = 10^{-4}$. *Solution at* $t = 0.05$ *for FSI (left) and FSI*1 *(right). From top to bottom, density, mean velocity, and temperature.*

Copyright © by SIAM. Unauthorized reproduction of this article is prohibited.

6. Conclusions. In this paper we have extended the hybrid kinetic methods developed in [13] to the case of an arbitrary fluid solver for the equilibrium component. Although the simplified BGK collision operator has been used to develop the schemes, extensions to the full Boltzmann operator of rarefied gas dynamics in principle are possible by using time relaxed methods [22, 25]. We plan to extend the schemes to the full Boltzmann equation in the near future.

The results obtained are very promising in terms of computational cost when compared to traditional deterministic methods for kinetic equations like the discrete velocity model or spectral schemes [19, 26]. In addition, the FSI hybrid algorithms yield fewer fluctuations than direct simulation Monte Carlo methods, and, close to the fluid regime, they permit faster computation of results. A remarkable feature of the FSI1 scheme is that the equilibrium fraction is essentially independent on the choice of the time step and thus provides more accurate results than Monte Carlo methods, even in resolved regimes.

Some open questions remain on alternative ways to estimate and increase the fraction of equilibrium in each space cell without increasing the computational cost. It is also interesting, and will be the subject of future work, to measure the response of the FSI hybrid methods in other situations such as simulations of nanosystem devices, plasma physics problems, or turbulence.

Acknowledgments. The authors would like to thank Russ Caflisch and Pierre Degond for several stimulating discussions.

REFERENCES

[1] P. L. Bhatnagar, E. P. Gross, and M. Krook, *A model for collision processes in gases.* I. *Small amplitude processes in charged and neutral one-component systems*, Phys. Rev., 94 (1954), pp. 511–525.

[2] G. A. Bird, *Molecular Gas Dynamics and Direct Simulation of Gas Flows*, Clarendon Press, Oxford, UK, 1994.

[3] J. F. Bourgat, P. LeTallec, B. Perthame, and Y. Qiu, *Coupling Boltzmann and Euler equations without overlapping*, in Domain Decomposition Methods in Science and Engineering, Contemp. Math. 157, AMS, Providence, RI, 1994, pp. 377–398.

[4] R. E. Caflisch, *Monte Carlo and quasi-Monte Carlo methods*, in Acta Numer. 7, Cambridge University Press, Cambridge, UK, 1998, pp. 1–49.

[5] C. Cercignani, *The Boltzmann Equation and Its Applications*, Springer-Verlag, New York, 1988.

[6] C. Cercignani, *Rarefied Gas Dynamics: From Basic Concepts to Actual Calculations*, Cambridge Texts Appl. Math., Cambridge University Press, Cambridge, UK, 2000.

[7] F. Coron and B. Perthame, *Numerical passage from kinetic to fluid equations*, SIAM J. Numer. Anal., 28 (1991), pp. 26–42.

[8] N. Crouseilles, P. Degond, and M. Lemou, *A hybrid kinetic-fluid model for solving the gas-dynamics Boltzmann BGK equation*, J. Comput. Phys., 199 (2004), pp. 776–808.

[9] P. Degond, G. Dimarco, and L. Mieussens, *A moving interface method for dynamic kinetic-fluid coupling*, J. Comput. Phys., 227 (2007), pp. 1176–1208.

[10] P. Degond, S. Jin, and L. Mieussens, *A smooth transition between kinetic and hydrodynamic equations*, J. Comput. Phys., 209 (2005), pp. 665–694.

[11] S. Deshpande, *A Second Order Accurate Kinetic Theory Based Method for Inviscid Compressible Flow*, NASA Langley Technical paper 2613, Langley Research Center, Hampton, VA, 1986.

[12] G. Dimarco and L. Pareschi, *Hybrid multiscale methods* I. *Hyperbolic relaxation problems*, Comm. Math. Sci., 1 (2006), pp. 155–177.

[13] G. Dimarco and L. Pareschi, *Hybrid multiscale methods* II. *Kinetic equations*, Multiscale Model. Simul., 6 (2008), pp. 1169–1197.

[14] G. Dimarco and L. Pareschi, *Domain decomposition techniques and hybrid multiscale methods for kinetic equations*, in Proceedings of the 11th International Conference on Hyperbolic

Copyright © by SIAM. Unauthorized reproduction of this article is prohibited.

Problems: Theory, Numerics, Applications, Lyon, France, 2006, Springer, New York, 2008, pp. 457–464.
[15] W. E and B. Engquist, *The heterogeneous multiscale methods*, Comm. Math. Sci., 1 (2003), pp. 87–133.
[16] W. E and B. Engquist, *Multiscale Modeling and Computation*, Notices Amer. Math. Sci., 50 (2003), pp. 1062–1070.
[17] S. Jin, *Runge-Kutta methods for hyperbolic conservation laws with stiff relaxation terms*, J. Comput. Phys., 122 (1995), pp. 51–67.
[18] S. Jin and Z. P. Xin, *Relaxation schemes for systems of conservation laws in arbitrary space dimensions*, Comm. Pure Appl. Math., 48 (1995), pp. 235–276.
[19] L. Mieussens, *Discrete velocity model and implicit scheme for the BGK equation of rarefied gas dynamic*, Math. Models Methods Appl. Sci., 10 (2000), pp. 1121–1149.
[20] P. LeTallec and F. Mallinger, *Coupling Boltzmann and Navier–Stokes by half fluxes*, J. Comput. Phys., 136 (1997), pp. 51–67.
[21] S. Liu, *Monte Carlo Strategies in Scientific Computing*, Springer, New York, 2004.
[22] L. Pareschi and R. E. Caflisch, *Implicit Monte Carlo methods for rarefied gas dynamics* I: *The space homogeneous case*, J. Comput. Phys., 154 (1999), pp. 90–116.
[23] L. Pareschi and R. E. Caflisch, *Towards an hybrid method for rarefied gas dynamics*, IMA Vol. Math. Appl., 135 (2004), pp. 57–73.
[24] L. Pareschi and S. Trazzi, *Numerical solution of the Boltzmann equation by time relaxed Monte Carlo (TRMC) methods*, Internat. J. Numer. Methods Fluids, 48 (2005), pp. 947–983.
[25] L. Pareschi and G. Russo, *Time relaxed Monte Carlo methods for the Boltzmann equation*, SIAM J. Sci. Comput., 23 (2001), pp. 1253–1273.
[26] L. Pareschi and G. Russo, *Numerical solution of the Boltzmann equation* I: *Spectrally accurate approximation of the collision operator*, SIAM J. Numer. Anal., 37 (2000), pp. 1217–1245.
[27] L. Pareschi, *Hybrid multiscale methods for hyperbolic and kinetic problems*, in ESAIM Proc. 15, T. Goudon, E. Sonnendrucker, and D. Talay, eds., SMAI, Paris, 2005, pp. 87–120.
[28] B. Perthame, *Boltzmann type schemes for gas dynamics and the entropy property*, SIAM J. Numer. Anal., 27 (1990), pp. 1405–1421.
[29] B. Perthame, *Second-order Boltzmann schemes for compressible Euler equations in one and two space dimensions*, SIAM J. Numer. Anal., 29 (1992), pp. 1–19.
[30] S. Pieraccini and G. Puppo, *Implicit-explicit schemes for BGK kinetic equations*, J. Sci. Comput., 32 (2007), pp. 1–28.
[31] D. I. Pullin, *Generation of normal variates with given sample*, J. Statist. Comput. Simul., 9 (1979), pp. 303–309.
[32] R. Roveda, D. B. Goldstein, and P. L. Varghese, *Hybrid Euler/direct simulation Monte Carlo calculation of unsteady slit flow*, AIAA J. Spacecraft Rockets, 37 (2000), pp. 753–760.
[33] S. Tiwari, *Coupling of the Boltzmann and Euler equations with automatic domain decomposition*, J. Comput. Phys., 144 (1998), pp. 710–726.
[34] K. Xu, *A gas-kinetic BGK scheme for the Navier–Stokes equations and its connection with artificial dissipation and Godunov method*, J. Comput. Phys., 171 (2001), pp. 289–335.

Copyright © by SIAM. Unauthorized reproduction of this article is prohibited.